NAVAL POSTGRADUATE SCHOOL

MONTEREY, CALIFORNIA

THESIS

RECIPROCITY IN VECTOR ACOUSTICS

by

Thomas J. Deal

March 2017

Thesis Advisor: Kevin B. Smith
Second Reader: Benjamin Cray

Approved for public release. Distribution is **unlimited.**

Reissued 30 May 2017 with Second Reader's non-NPS affiliation added to title page.

THIS PAGE INTENTIONALLY LEFT BLANK

REPORT DOCUMENTATION PAGE

Form Approved OMB No. 0704–0188

1. AGENCY USE ONLY *(Leave Blank)*	2. REPORT DATE	3. REPORT TYPE AND DATES COVERED
	March 2017	Master's Thesis 07-01-2014 to 03-31-2017

4. TITLE AND SUBTITLE

RECIPROCITY IN VECTOR ACOUSTICS

5. FUNDING NUMBERS

6. AUTHOR(S)

Thomas J. Deal

7. PERFORMING ORGANIZATION NAME(S) AND ADDRESS(ES)

Naval Postgraduate School
Monterey, CA 93943

8. PERFORMING ORGANIZATION REPORT NUMBER

9. SPONSORING / MONITORING AGENCY NAME(S) AND ADDRESS(ES)

N/A

10. SPONSORING / MONITORING AGENCY REPORT NUMBER

11. SUPPLEMENTARY NOTES

The views expressed in this document are those of the author and do not reflect the official policy or position of the Department of Defense or the U.S. Government. IRB Protocol Number: N/A.

12a. DISTRIBUTION / AVAILABILITY STATEMENT

Approved for public release. Distribution is unlimited.

12b. DISTRIBUTION CODE

13. ABSTRACT *(maximum 200 words)*

The scalar reciprocity equation commonly stated in underwater acoustics relates pressure fields and monopole sources. It is often used to predict the pressure measured by a hydrophone for multiple source locations by placing a source at the hydrophone location and calculating the field everywhere for that source. That method, however, does not work when calculating the orthogonal components of the velocity field measured by a fixed receiver. This thesis derives a vector-scalar reciprocity equation that accounts for both monopole and dipole sources. This equation can be used to calculate individual components of the received vector field by altering the source type used in the propagation calculation. This enables a propagation model to calculate the received vector field components for an arbitrary number of source locations with a single model run for each received field component instead of requiring one model run for each source location. Application of the vector-scalar reciprocity principle is demonstrated with analytic solutions for a range-independent environment and with numerical solutions for a range-independent and a range-dependent environment using a parabolic equation model.

14. SUBJECT TERMS

reciprocity, vector field, parabolic equation, acoustic dipole

15. NUMBER OF PAGES 65

16. PRICE CODE

17. SECURITY CLASSIFICATION OF REPORT	18. SECURITY CLASSIFICATION OF THIS PAGE	19. SECURITY CLASSIFICATION OF ABSTRACT	20. LIMITATION OF ABSTRACT
Unclassified	Unclassified	Unclassified	UU

NSN 7540-01-280-5500

Standard Form 298 (Rev. 2–89)
Prescribed by ANSI Std. 239–18

THIS PAGE INTENTIONALLY LEFT BLANK

Approved for public release. Distribution is **unlimited.**

RECIPROCITY IN VECTOR ACOUSTICS

Thomas J. Deal
Electronics Engineer, Naval Undersea Warfare Center
M.S.E.E., Rensselaer Polytechnic Institute, 2001
B.S.E.E., University of Alabama, 2000

Submitted in partial fulfillment of the
requirements for the degree of

MASTER OF SCIENCE IN ENGINEERING ACOUSTICS

from the

NAVAL POSTGRADUATE SCHOOL
March 2017

Approved by: Kevin B. Smith
Thesis Advisor

Benjamin Cray, Naval Undersea Warfare Center Division Newport
Second Reader

Daphne Kapolka
Chair, Engineering Acoustics Academic Committee

THIS PAGE INTENTIONALLY LEFT BLANK

ABSTRACT

The scalar reciprocity equation commonly stated in underwater acoustics relates pressure fields and monopole sources. It is often used to predict the pressure measured by a hydrophone for multiple source locations by placing a source at the hydrophone location and calculating the field everywhere for that source. That method, however, does not work when calculating the orthogonal components of the velocity field measured by a fixed receiver. This thesis derives a vector-scalar reciprocity equation that accounts for both monopole and dipole sources. This equation can be used to calculate individual components of the received vector field by altering the source type used in the propagation calculation. This enables a propagation model to calculate the received vector field components for an arbitrary number of source locations with a single model run for each received field component instead of requiring one model run for each source location. Application of the vector-scalar reciprocity principle is demonstrated with analytic solutions for a range-independent environment and with numerical solutions for a range-independent and a range-dependent environment using a parabolic equation model.

THIS PAGE INTENTIONALLY LEFT BLANK

Table of Contents

THIS PAGE INTENTIONALLY LEFT BLANK

List of Figures

List of Tables

THIS PAGE INTENTIONALLY LEFT BLANK

Acknowledgments

I dedicate this thesis to my wife, Sally, and my children, Laura, Jessica, and Alexander. Thank you for being willing to uproot your lives and move across the country to support me during my time at NPS.

THIS PAGE INTENTIONALLY LEFT BLANK

CHAPTER 1:
Introduction

The principle of acoustic pressure reciprocity, originally developed by Lord Rayleigh [1], is a simple yet powerful statement that has found many applications, particularly in the area of propagation modeling. The relationship is governed by

$$\frac{p_1(\mathbf{r}_2)}{\rho(\mathbf{r}_2)} = \frac{p_2(\mathbf{r}_1)}{\rho(\mathbf{r}_1)} \tag{1.1}$$

where $\rho(\boldsymbol{r}_1)$ is the density at point $\boldsymbol{r}_1$ and $p_1(\boldsymbol{r}_2)$ is the Green's function at point $\boldsymbol{r}_2$ given a source at point $\boldsymbol{r}_1$. For the acoustic linear wave equation, the Green's function is related to the solution of the acoustic potential function, or the pressure field, due to omnidirectional point sources and receivers.

By relating the pressure received at one point in an acoustic field due to a source at another point to the pressure received when source and receiver positions are exchanged, the scalar reciprocity relationship allows two-way active propagation calculations to use the same path for the return echo that was calculated for the outgoing waveform. It also allows one-way passive calculations to determine the pressure received from multiple source locations by computing the acoustic field for a source at the receiver location. These and other applications of the reciprocity principle greatly reduce the computations required to predict hydrophone performance. There are some conditions for which reciprocity does not hold, i.e., in the presence of ocean currents, but despite those exceptions it remains a useful tool for the acoustician.

While hydrophones are only capable of measuring the scalar pressure field, vector sensors are able to measure the directional components of acceleration, velocity, or displacement. These components of the acoustic field contain information that is lost in the scalar pressure field, and exploiting that information requires the ability to model acoustic vector fields. In order to predict the performance of a vector sensor, one must be able to calculate the vector field components received by that sensor for any source position in an arbitrary, range-dependent environment. This application would be greatly simplified by invoking acoustic reciprocity, but the equation for reciprocity commonly given in textbooks holds only for

scalar fields such as pressure and velocity potential. The equation is not valid for velocity field components, which are proportional to the gradient of the potential field. Therefore, one cannot simply calculate the vector field for a point source and assume those vector quantities are what would be received by a vector sensor located at the source position.

However, as Rayleigh noted in regard to the principle of reciprocity, "apparent exceptions depend on a misunderstanding of the principle itself," and the failure of the scalar reciprocity equation to correctly give the directional components of vector fields is simply a misapplication of reciprocity. In fact, a vector-scalar reciprocity equation can be derived that accurately predicts the received vector fields for any source location in an arbitrary, range-dependent environment. That vector-scalar reciprocity relationship can be incorporated into propagation models and used just as the scalar reciprocity relationship has been.

This thesis demonstrates in Chapter 2 that the scalar reciprocity relationship works for pressure fields but not for velocity fields. It then derives the vector-scalar reciprocity equation in Chapter 3 and shows that it correctly calculates received vector fields in Chapter 4. The conclusion in Chapter 5 summarizes the results and outlines additional ways the vector reciprocity relationship can be used.

CHAPTER 2:
Limitations of the Scalar Reciprocity Equation

It is tempting to extend the reciprocal method for calculating received pressure fields to models that calculate directional field components such as vertical and radial displacement and velocity. However, this approach breaks down because while the reciprocity relationship as stated does hold for the displacement and velocity *potentials*, which are proportional to acoustic pressure, it does not hold for their individual components, which are proportional to the pressure gradient. This will be demonstrated with three examples: analytic expressions for normal modes in a range-independent environment, numerical results for that same environment, and numerical results for a range-dependent environment. The text, table, and figures in Sections 2.1 and 2.2 are adapted from [2].[1]

2.1 Analytic Expressions for Pressure and Particle Velocity in a Range-Independent Environment

The acoustic field of a point source in a range-independent waveguide has a closed-form solution that demonstrates which components of the vector field obey reciprocity. The pressure takes the form [3]

$$p(r,z) = \frac{j}{4\rho_0}\sum_{m=1}^{\infty}\Psi_m(z_s)\Psi_m(z)H_0^{(1)}(k_{rm}r), \tag{2.1}$$

where $\Psi_m(z)$ is the normalized mode shape function for the m^{th} normal mode propagating with horizontal wavenumber k_{rm}. This function depends on source depth, z_s, receiver depth, z, and the horizontal distance between them, r. Exchanging the source depth with

[1]Reprinted, with permission, from T. J. Deal and K. B. Smith, "Modeling acoustic vector fields for inverse problems," in *Proc. 2016 IEEE/OES China Ocean Acoustics*, Jan. 2016. This publication is a work of the U.S. Government as defined in Title 17, United States Code, Section 101. Copyright protection is not available for this work in the United States. IEEE will claim and protect its copyright in international jurisdictions where permission from IEEE must be obtained for all other uses, in any current or future media, including reprinting/republishing this material for advertising or promotional purposes, creating new collective works, for resale or redistribution to servers or lists, or reuse of any copyrighted component of this work in other works.

the receiver depth produces the same result for $p(r, z_s)$, satisfying the requirements of reciprocity.

Particle velocity can be calculated from pressure by computing the spatial gradient $\boldsymbol{v}(r, z) = \frac{1}{j\omega\rho_0}\nabla p(r, z)$. Its radial and vertical components are [4]

$$v_r(r, z) = \frac{-1}{4\omega\rho_0^2}\sum_{m=1}^{\infty}\Psi_m(z_s)\Psi_m(z)k_{rm}H_1^{(1)}(k_{rm}r), \tag{2.2}$$

$$v_z(r, z) = \frac{1}{4\omega\rho_0^2}\sum_{m=1}^{\infty}\Psi_m(z_s)\frac{\partial\Psi_m(z)}{\partial z}H_0^{(1)}(k_{rm}r). \tag{2.3}$$

Like pressure, the radial velocity v_r is unchanged when source and receiver depths exchange, so it also obeys reciprocity in this range-independent environment. However, Equation (2.3) has different dependence on the source and receiver depths. Unless the mode shape function is proportional to its first derivative, vertical velocity does not obey reciprocity.

In a Pekeris waveguide with a fluid layer of depth h, sound speed c, and density ρ bounded by a pressure release surface and semi-infinite fluid bottom with sound speed c_b and density ρ_b, the mode shape function is

$$\Psi_m(z) = A_m \sin\left(k_{zm}z\right), \qquad 0 \le z \le h, \tag{2.4}$$

where k_{zm} is the vertical wavenumber for the m^{th} mode in the fluid layer. The mode normalization factor A_m is given by [5]

$$A_m^{-2} = \frac{h}{2\rho_0}\left[1 - \frac{\sin\left(2k_{zm}h\right)}{2k_{zm}h} + j\frac{\rho_0}{\rho_b}\frac{\sin^2\left(k_{zm}h\right)}{k_{bzm}h}\right], \tag{2.5}$$

where k_{bzm} is the vertical wavenumber for the m^{th} mode in the bottom halfspace. The pressure field can then be expressed as

$$p(r, z) = \frac{j}{4\rho_0}\sum_{m=1}^{\infty}A_m^2\sin\left(k_{zm}z_s\right)\sin\left(k_{zm}z\right)H_0^{(1)}(k_{rm}r). \tag{2.6}$$

The mode shape's vertical derivative is

$$\frac{\partial \Psi_m(z)}{\partial z} = k_{zm} A_m \cos\left(k_{zm} z\right), \tag{2.7}$$

so the expressions for the radial and vertical velocity become

$$v_r(r,z) = \frac{-1}{4\omega\rho_0^2} \sum_{m=1}^{\infty} A_m^2 \sin\left(k_{zm} z_s\right) \sin\left(k_{zm} z\right) k_{rm} H_1^{(1)}(k_{rm} r), \tag{2.8}$$

$$v_z(r,z) = \frac{1}{4\omega\rho_0^2} \sum_{m=1}^{\infty} A_m^2 \sin\left(k_{zm} z_s\right) \cos\left(k_{zm} z\right) k_{zm} H_0^{(1)}(k_{rm} r). \tag{2.9}$$

This mode shape function is 90 degrees out of phase with its derivative, so exchanging source and receiver positions will produce drastically different results for vertical velocity, but it will leave the radial velocity unchanged.

2.2 Numerical Solutions to the Range-Independent Environment

The acoustic vector field for the range-independent environment can be demonstrated by implementing the analytic equations for the normal modes with specific values for the environment and source parameters. The water layer is 200 m deep with sound speed 1500 m/s and density 1.0 g/cm^3. The bottom has sound speed 1700 m/s and density 1.5 g/cm^3. For a continuous source at 25 Hz, there will be seven trapped modes. This waveguide also supports higher order modes and a branch line integral, but their effect is limited to the region near the source, and the trapped modes dominate at ranges greater than a few water depths, so they are omitted here for clarity. The horizontal and vertical wavenumbers for the trapped modes are listed in Table 2.1.

These wavenumbers are used with Equations (2.6), (2.8), and (2.9) to generate the plots for pressure, radial velocity, and vertical velocity for both a fixed source and a fixed receiver in Figure 2.1. For the fixed source cases, the source is at a depth of 100 m and range of 0 km, and the field components are calculated for all receiver ranges and depths. For the fixed receiver cases, the receiver is at a depth of 100 m and range of 0 km, and the field components are calculated from all combinations of source depths and ranges. In

Table 2.1. Horizontal and vertical wavenumbers of trapped modes for 25 Hz source in example Pekeris waveguide. Source: [2].

Mode m	k_{rm}	k_{zm}
1	0.1038 + 0.0000i	0.0137 + 0.0000i
2	0.1011 + 0.0000i	0.0275 + 0.0000i
3	0.0962 + 0.0000i	0.0413 + 0.0000i
4	0.0893 + 0.0009i	0.0548 - 0.0015i
5	0.0774 + 0.0024i	0.0706 - 0.0026i
6	0.0595 + 0.0045i	0.0863 - 0.0031i
7	0.0269 + 0.0127i	0.1021 - 0.0033i

this way, the fixed source fields represent the response due to a single source location, as a function of range and depth, and the fixed receiver fields are a function of source range and depth, representing the response from a mobile source location as observed at a single, fixed receiver.

Computing these fields using the analytic expressions is straightforward because they are formulated as a function of r, z, and z_s, and any two of these parameters may be varied to create a two-dimensional plot with the third parameter held constant. However, many propagation models only compute the field as a function of r and z for a fixed z_s. Using these models to calculate the fixed receiver field is more complicated. A source is placed at a point (r, z_s) in the waveguide. The geometry is then shifted horizontally such that the source is located at a range of zero and the receiver is a distance r away. The propagation model is run, and its solutions for field components are evaluated at the receiver location (r, z), where receiver depth z is fixed. The pressure and velocity components measured at this fixed receiver position are plotted at the source location (r, z_s). This process is repeated for all source locations until the entire field is completed with the required range and depth resolution. In this way, the fixed receiver plots indicate the pressure and velocity response due to a source located at each point in the field.

All pressure plots are in decibels of transmission loss referenced to one Pascal at one meter for a monopole with source strength of one Pascal at one meter. This provides a normalized transmission loss of zero dB at one meter. Velocity plots are in decibels referenced to one meter per second for the same source strength. Contours are drawn at five dB increments.

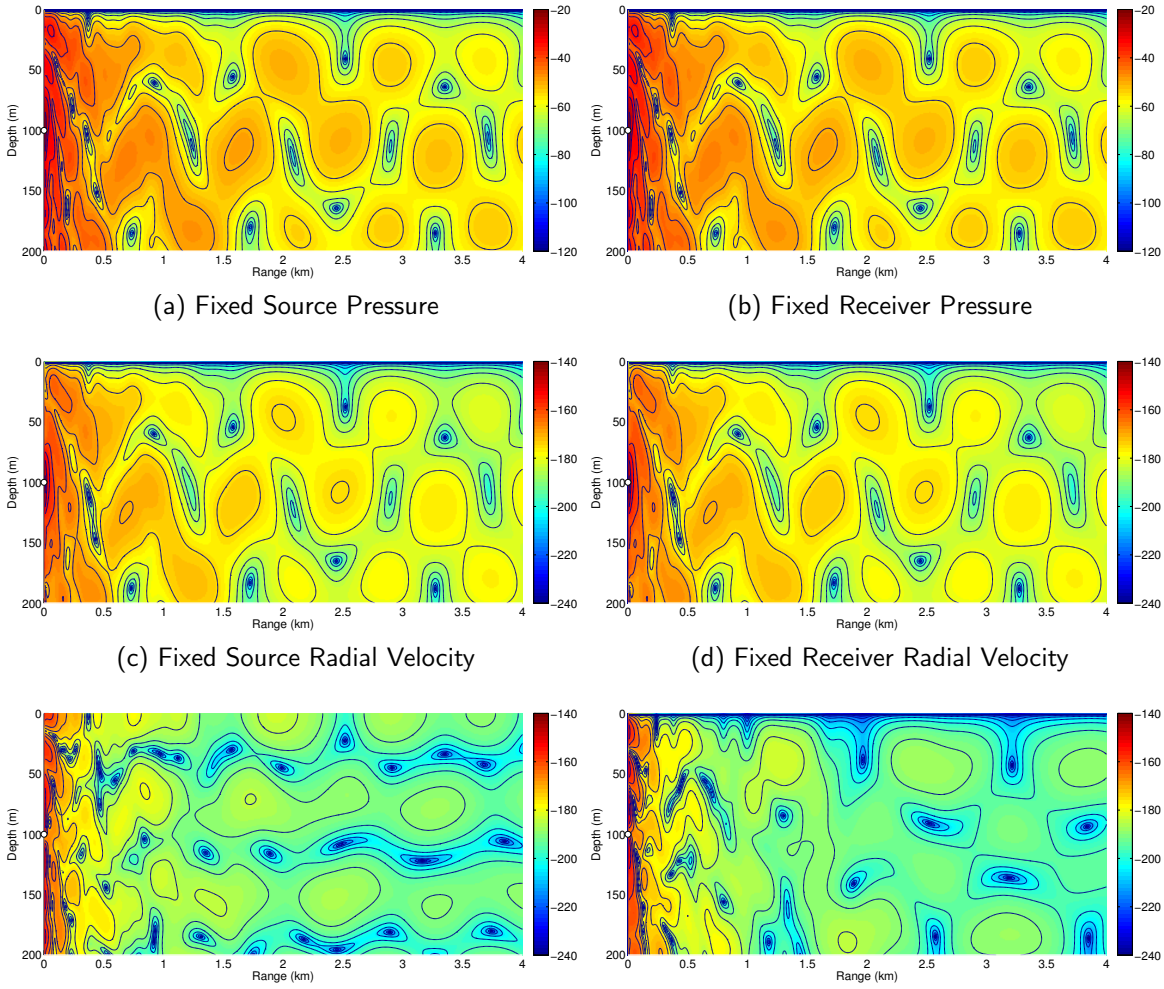

(a) Fixed Source Pressure

(b) Fixed Receiver Pressure

(c) Fixed Source Radial Velocity

(d) Fixed Receiver Radial Velocity

(e) Fixed Source Vertical Velocity

(f) Fixed Receiver Vertical Velocity

Figure 2.1. Vector field components in the Pekeris waveguide calculated from analytic expressions for trapped modes using scalar reciprocity. Pressure is in dB//1Pa. Velocity is in dB//1m/s. Transmission loss contours are drawn every 5 dB. Adapted from [2].

As seen in Figure 2.1a and Figure 2.1b, the pressure field is identical when source and receiver positions are exchanged. The same is true for the radial velocity in Figure 2.1c and

Figure 2.1d. However, the vertical velocity plots are completely different. The field for the fixed source has vertical velocity nodes around 40 and 120 meters that are consistent with range, while the vertical velocity nodes for the fixed receiver show no such consistency with range. The fields at zero depth are also significantly different, with the fixed source field having maxima for receivers at the surface and the fixed receiver field having minima for sources at the surface.

The Monterey-Miami Parabolic Equation (MMPE) model [6] is used to further demonstrate the differences in the field components for a fixed source and a fixed receiver. It correctly captures the effects of leaky modes and the lateral wave, and it also supports range-dependent calculations. The fixed source case requires a single run of MMPE, while the fixed receiver case requires one run for each source range and depth in the field. Figure 2.2 shows the pressure, radial velocity, and vertical velocity for a fixed source and fixed receiver in the example Pekeris waveguide.

As seen in Figure 2.2a and Figure 2.2b, the pressure field is identical when source and receiver positions are exchanged, even in the near field where the lateral wave and leaky modes have greater influence. Beyond 2.5 km the pressure field settles into the far field pattern predicted by Equation (2.6). The same is true for the radial velocity in Figure 2.2c and Figure 2.2d. However, the vertical velocity plots are again significantly different. This is true both in the near field and far field. In all cases, the results from MMPE are in excellent agreement with the analytic solution for the Pekeris waveguide, with the exception of the near-field components that were not included in the trapped mode solution.

Figures 2.3–2.5 quantify the error between the reciprocal fields calculated with MMPE using a monopole source at the receiver location and the reference fields calculated by moving the monopole source throughout the water column. Magnitude difference is measured in decibels, so it is effectively the ratio between the two fields' magnitudes and will be zero dB when they are equal. Phase error is the phase angle of the reciprocal field minus the phase angle of the reference field measured in degrees. The histograms for magnitude and phase error use 1 dB and 1 degree bins for all the computed range and depth data points to display the distribution of errors. The histogram bin amplitudes have been divided by the total number of field points in the calculation to normalize them. If the error was exactly zero everywhere, the histograms would have a single bar at horizontal coordinate zero and

amplitude 1. Box plots quantify the statistics of these distributions by displaying the mean, lower quartile, and upper quartile.

In addition to the error plots, first and second order moments are calculated over all data points in the water column. For phase errors, the mean and standard deviation are computed in degrees. For magnitude errors, the mean and standard deviation are computed in dimensionless percent error instead of dB.

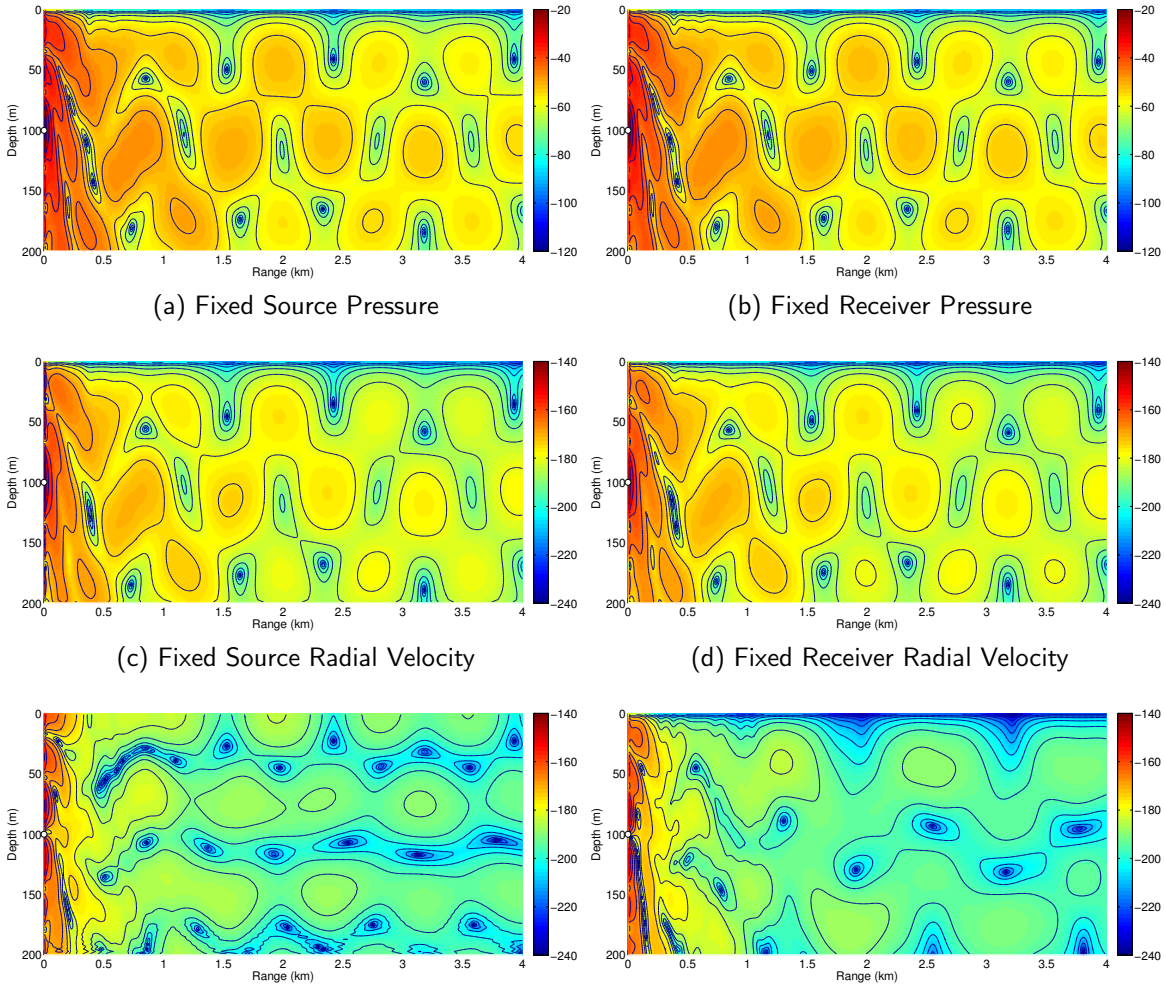

(a) Fixed Source Pressure

(b) Fixed Receiver Pressure

(c) Fixed Source Radial Velocity

(d) Fixed Receiver Radial Velocity

(e) Fixed Source Vertical Velocity

(f) Fixed Receiver Vertical Velocity

Figure 2.2. Vector field components in the Pekeris waveguide calculated with MMPE using scalar reciprocity. Pressure is in dB//1Pa. Velocity is in dB//1m/s. Transmission loss contours are drawn every 5 dB. Adapted from [2].

As expected, the reciprocal pressure field matches well with the reference field. The error magnitude mean is 0.618%, and the error magnitude standard deviation is 10.0%. The phase error mean is -0.0501 degrees, and its standard deviation is 3.28 degrees. The points in the field with the greatest magnitude and phase errors correspond to nulls in the pressure field, which are caused by destructive interference. At these points the pressure magnitude is 40-60 dB lower than points nearby, so errors in the field have little impact on calculations such as transmission loss.

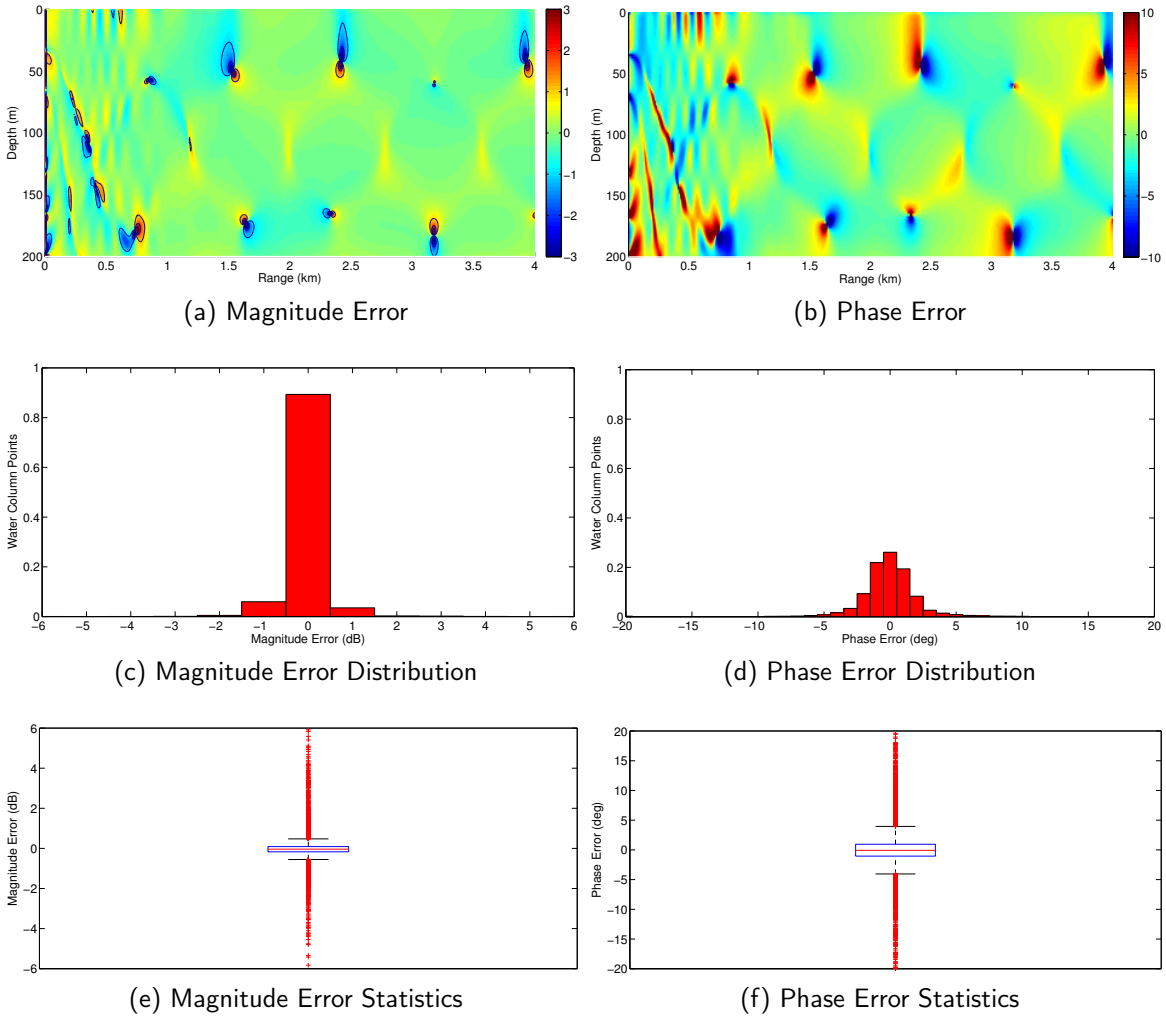

(a) Magnitude Error

(b) Phase Error

(c) Magnitude Error Distribution

(d) Phase Error Distribution

(e) Magnitude Error Statistics

(f) Phase Error Statistics

Figure 2.3. Computational error calculating the received pressure field in the Pekeris waveguide using MMPE and scalar reciprocity. Magnitude error contours are drawn for ±1, ±2, and ±3 dB.

For the range-independent Pekeris waveguide, Equation (2.8) predicts that the radial velocity field should be reciprocal, and that is supported by the error plots in Figure 2.4. The magnitude error mean is 0.321%, and the standard deviation is 10.9%. The phase error mean is 0.0222 degrees, and the standard deviation is 3.73 degrees. These numbers are in good agreement with the statistics for pressure error.

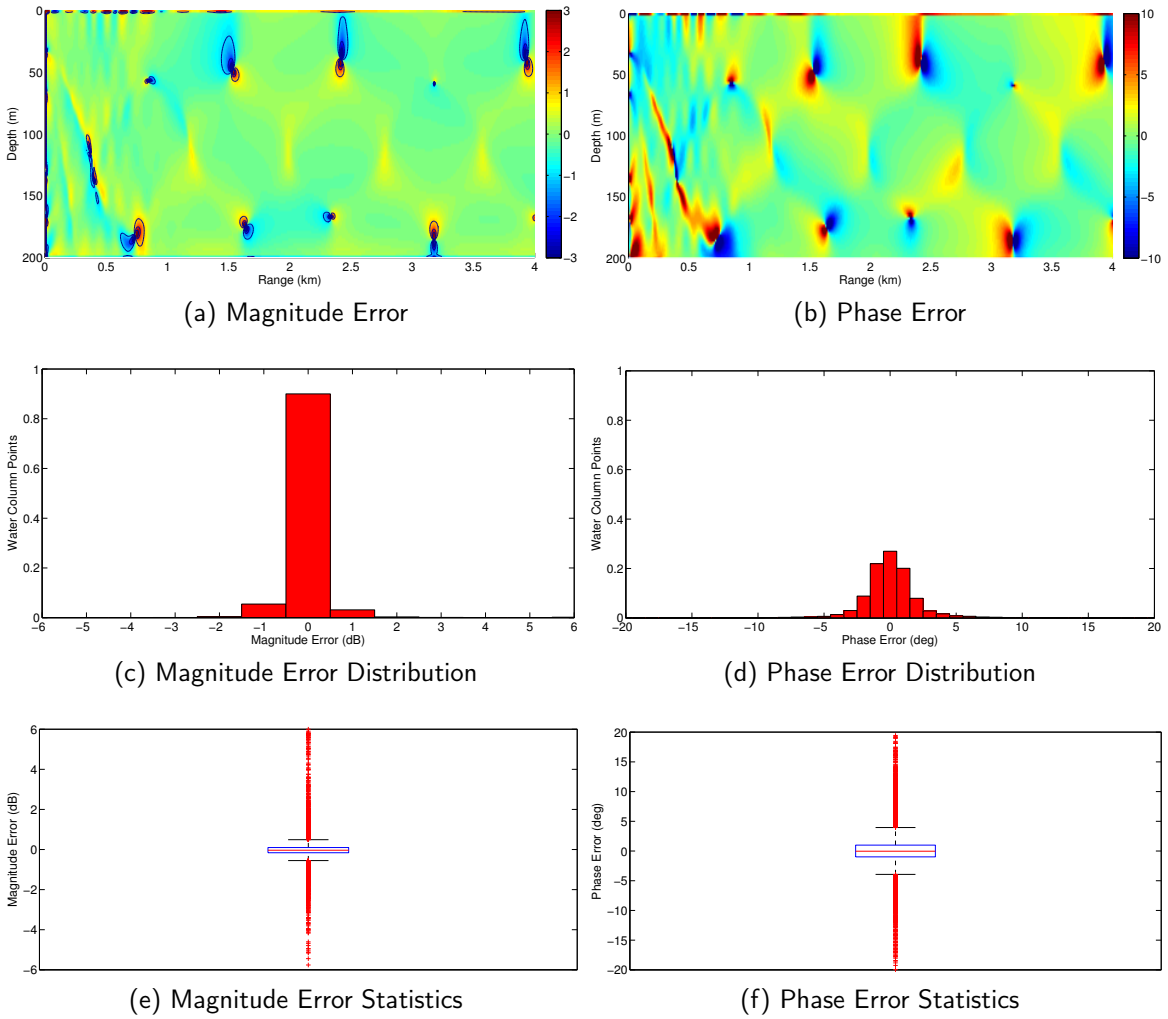

(a) Magnitude Error

(b) Phase Error

(c) Magnitude Error Distribution

(d) Phase Error Distribution

(e) Magnitude Error Statistics

(f) Phase Error Statistics

Figure 2.4. Computational error calculating the received radial velocity field in the Pekeris waveguide using MMPE and scalar reciprocity. Magnitude error contours are drawn for ±1, ±2, and ±3 dB.

The reciprocal calculation for vertical velocity, however, is a poor match for the reference solution at almost all ranges and depths, as shown in Figure 2.5. Note that the vertical axes on the histograms in Figures 2.5c and 2.5d and box plots in Figures 2.5e and 2.5f have been expanded compared to the histograms and box plots for pressure and radial velocity due to the large error spread for vertical velocity. The magnitude error mean is 105%, and the high standard deviation of 945% shows that the errors have a large spread. The phase error mean is low at 0.657 degrees, but the standard deviation is 99.6 degrees, which indicates the low mean is due to an even spread of large phase errors rather than a tight group of low phase errors. The one exception to the large magnitude and phase errors lies on the line where the source depth is equal to the receiver depth. It is only at this depth that the vertical velocity given by Equation (2.9) is the same when source and receiver positions are interchanged. It will be shown that this result does not hold in range-dependent environments.

The error statistics for calculating the reciprocal pressure and velocity field components are summarized in Table 2.2. Distilling values calculated over an entire field into a single number tends to obscure the details of how well the calculations do or do not match, but in this instance, the standard deviation values provide good insight into which reciprocal calculations perform better.

Table 2.2. Vector field calculation error statistics using scalar reciprocity for a monopole source in the Pekeris waveguide

		Pressure	Radial Velocity	Vertical Velocity
Magnitude (%)	mean	0.618	0.321	105
	std	10.0	10.9	945
Phase (deg)	mean	-0.0501	0.0222	0.657
	std	3.28	3.73	99.6

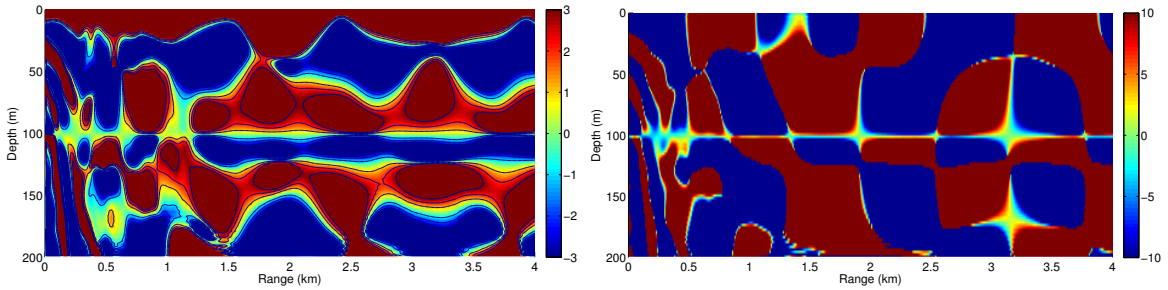

(a) Magnitude Error

(b) Phase Error

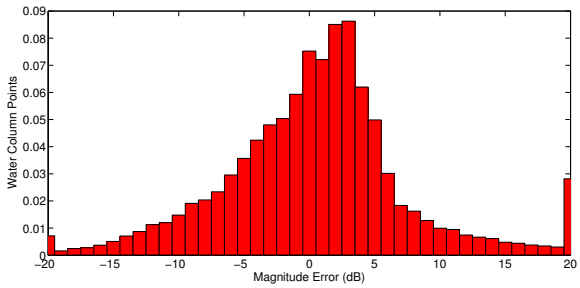

(c) Magnitude Error Distribution

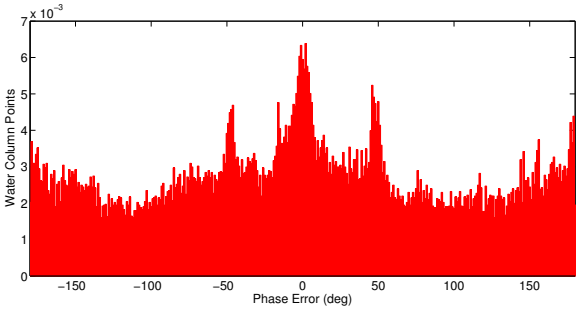

(d) Phase Error Distribution

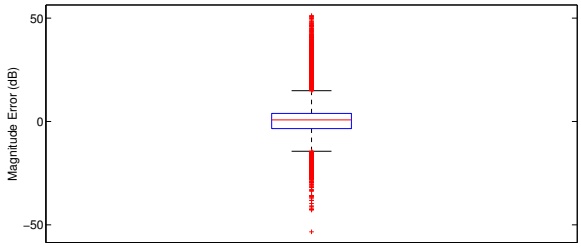

(e) Magnitude Error Statistics

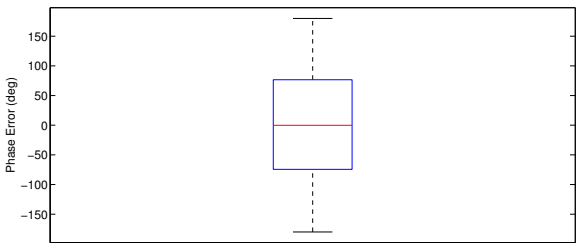

(f) Phase Error Statistics

Figure 2.5. Computational error calculating the received vertical velocity field in the Pekeris waveguide using MMPE and scalar reciprocity. Magnitude error contours are drawn for ±1, ±2, and ±3 dB.

2.3 Numerical Solutions to the Range-Dependent Environment

The shelf break test case from the SWAM '99 workshop [7] provides varying bathymetry and sound speed that is useful for demonstrating the limitations of the scalar reciprocity equation for predicting vector fields in an arbitrary environment, as shown in Figure 2.6. The water has constant density of 1.0 g/cm^3, and the bottom is homogeneous with sound speed 1700 m/s, density 1.5 g/cm^3, compressional attenuation 0.1 dB/λ, and no shear. The range-dependent bathymetry has depth

$$z_b = \begin{cases} 100, & r \leq 5000 \\ \frac{1}{50}r, & 5000 < r \leq 20000, \end{cases} \tag{2.10}$$

where z_b and r are in meters. For depths $z < z_b$, the water sound speed in m/s is defined by

$$c(r, z) = 1450 + 4.6T(r, z) - 0.055T^2(r, z) + 0.016z \tag{2.11}$$

where $T(r, z)$ is the temperature in degrees Celsius defined by

$$T(r, z) = 5 + T_0(r)\left(\frac{\sinh\left(\frac{\pi(400-z)}{200}\right)}{265}\right)^2 \tag{2.12}$$

with the surface temperature in degrees Celsius defined by

$$T_0(r) = 15 - 5\left(1 + \tanh(10 - \frac{r}{1000})\right). \tag{2.13}$$

This SWAM'99 environment was intended to represent a canonical shelf break environment. The receiver is located on the shelf in the water column at a depth of 35 m and range of 0 m. The goal is to calculate the vector field received by that sensor for a 25 Hz monopole source located at any depth in the water column for ranges from 0 km to 20 km.

The vector field components are plotted in Figure 2.7. On the right are the reference solutions calculated by placing a monopole source at each location in the field and computing the pressure and velocity at the fixed receiver position on the shelf. On the left are the pressure and velocity at each point in the field for a monopole source on the shelf.

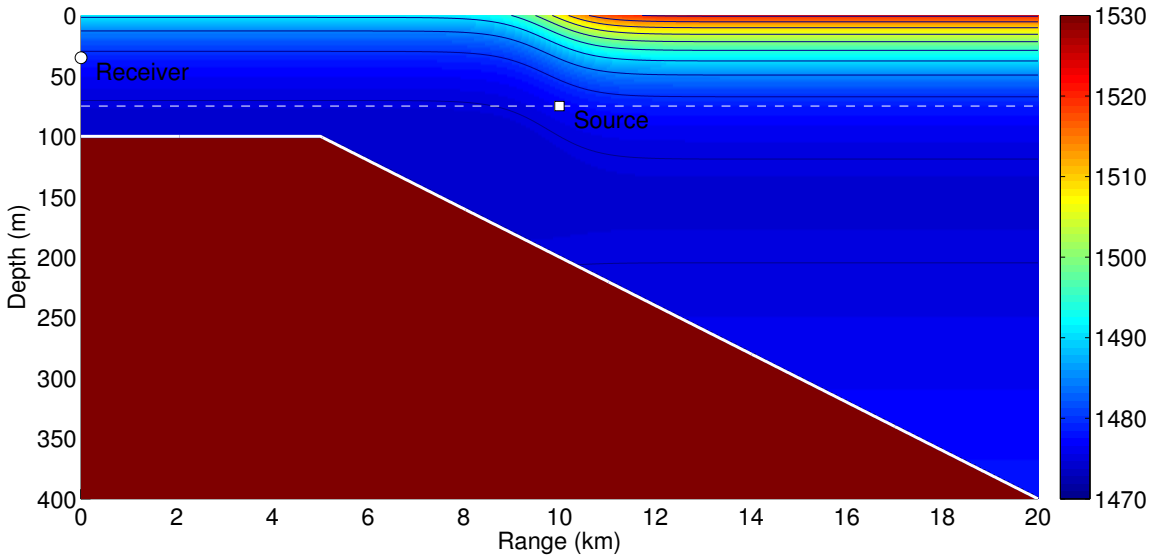

Figure 2.6. Range-dependent geometry showing fixed receiver location, variable-range source depth, bathymetry, and sound speed profile. Sound speed contours are drawn every 5 m/s.

Figure 2.8 shows the error in estimating the received pressure field using the reciprocal method with a monopole source. As expected, there is excellent agreement between the reciprocal method and the reference solution. In fact, it is this excellent agreement in highly range-dependent environments, along with the significant computational savings achieved, which makes the reciprocal pressure calculation so popular. Pressure error magnitude for all data points in the water column has a mean of 1.85% and standard deviation of 31.1%, and the pressure phase error has a mean of -0.0228 degrees and standard deviation of 10.3 degrees. Further inspection of the error surfaces in Figure 2.8 indicates that the regions of greatest magnitude and phase error are at points close to nulls in the pressure field pattern. At these locations of destructive interference, the pressure magnitude is 40-60 dB less than the pressure at comparable ranges, so errors in the field calculation at these points are more easily tolerated in most applications.

The error in calculating the radial velocity using the reciprocal method with a monopole source is shown in Figure 2.9. There is generally good agreement between the reciprocal calculation and the reference solution at short ranges when both source and receiver are on the shelf and the environment is approximately range-independent. This is the behavior predicted by Equation (2.2) and seen in the Pekeris waveguide example. As the source

moves beyond the range where the bathymetry and sound speed profile begin to vary, the reciprocal solution begins to deviate from the reference solution. For all water column points, the magnitude error has a mean of 6.18% and a standard deviation of 51.9%, and the phase error has a mean of -0.405 degrees and a standard deviation of 12.4 degrees. As with the pressure field calculations, the locations of greatest error coincide with nulls in the radial velocity field due to destructive interference. While the average magnitude and phase errors that result from this reciprocal calculation may be tolerable for many applications,

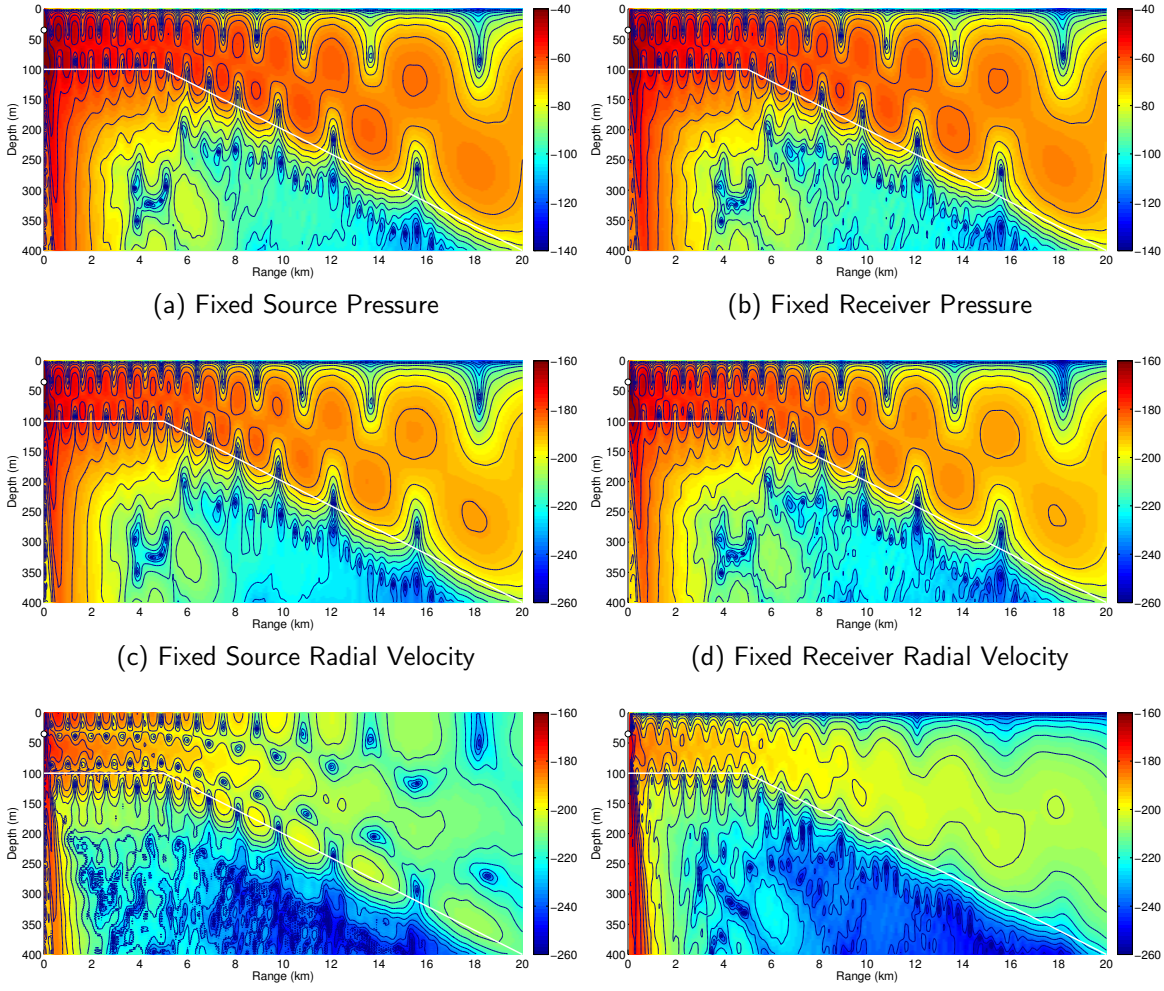

(a) Fixed Source Pressure

(b) Fixed Receiver Pressure

(c) Fixed Source Radial Velocity

(d) Fixed Receiver Radial Velocity

(e) Fixed Source Vertical Velocity

(f) Fixed Receiver Vertical Velocity

Figure 2.7. Vector field components in the shelf break environment calculated with MMPE using scalar reciprocity. Pressure is in dB//1Pa. Velocity is in dB//1m/s. Transmission loss contours are drawn every 5 dB.

the trend of increasing error with range indicates a fundamental flaw in using a monopole source to predict received radial velocity.

The largest errors produced by this misapplication of the reciprocity theorem are evident in the vertical velocity fields, as shown in Figure 2.10. The vertical axes on the histograms in Figures 2.10c and 2.10d have been expanded due to the large error spread and consequent low bin amplitudes. The magnitude and phase for the reciprocal field are in poor agreement with the reference solution at most points in the field. This wide variation leads to magnitude

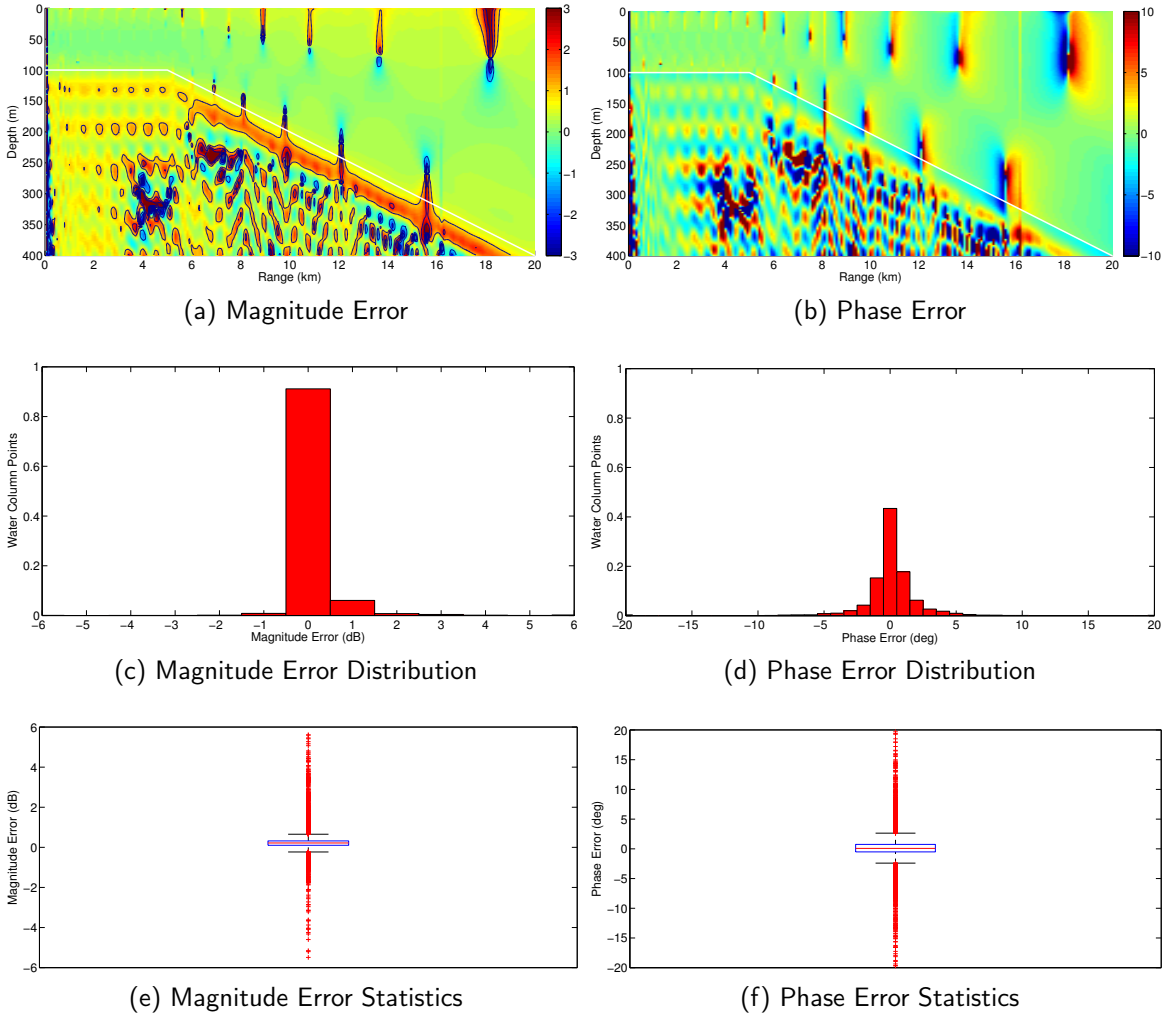

(a) Magnitude Error

(b) Phase Error

(c) Magnitude Error Distribution

(d) Phase Error Distribution

(e) Magnitude Error Statistics

(f) Phase Error Statistics

Figure 2.8. Computational error calculating the received pressure field in the shelf break environment using MMPE and scalar reciprocity. Magnitude error contours are drawn for ±1, ±2, and ±3 dB.

and phase error means of 20.1% and 0.261 degrees, but the standard deviations are much higher at 1340% and 98.7 degrees. As in the Pekeris waveguide example, there are low magnitude and phase errors for vertical velocity on the line where source depth equals receiver depth at short ranges where the source is still on the shelf and the environment is approximately range-independent. As the bathymetry and sound speed profile begin to change, this localized region of low error vanishes, so it is not a feature to be relied upon in range-dependent environments. Estimating the received vertical velocity field on the shelf

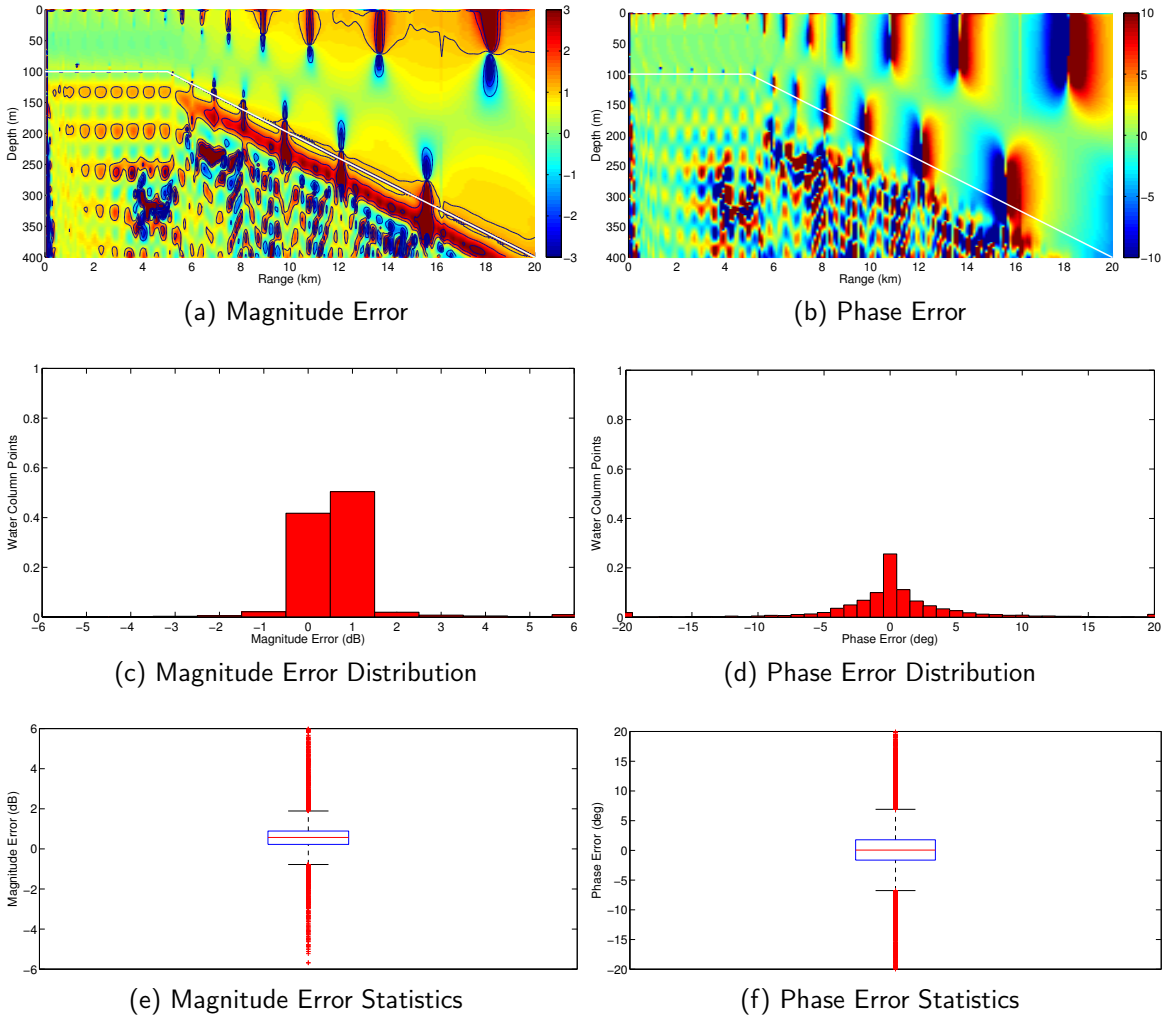

(a) Magnitude Error

(b) Phase Error

(c) Magnitude Error Distribution

(d) Phase Error Distribution

(e) Magnitude Error Statistics

(f) Phase Error Statistics

Figure 2.9. Computational error calculating the received radial velocity field in the shelf break environment using MMPE and scalar reciprocity. Magnitude error contours are drawn for ±1, ±2, and ±3 dB.

by calculating the vertical velocity received from a monopole source placed on the shelf is clearly incorrect.

The summary statistics for calculating the reciprocal pressure and velocity components for the range-dependent environment are shown in Table 2.3. The accumulating range errors in the radial velocity calculation are hidden in the single numbers for error mean and standard deviation, but the vertical velocity calculation errors are evident.

These examples demonstrate that the scalar reciprocity relationship, as stated in Equation 1.1, does not immediately extend to cover individual components of the vector field. Instead, a new reciprocity relationship must be derived that accounts for the spatial gradient of the pressure field.

Table 2.3. Vector field calculation error statistics using scalar reciprocity for a monopole source in the water column of the shelf break range-dependent environment

		Pressure	Radial Velocity	Vertical Velocity
Magnitude (%)	mean	1.85	6.18	20.1
	std	31.1	51.9	1340
Phase (deg)	mean	-0.0579	-0.334	6.41
	std	7.78	11.4	103

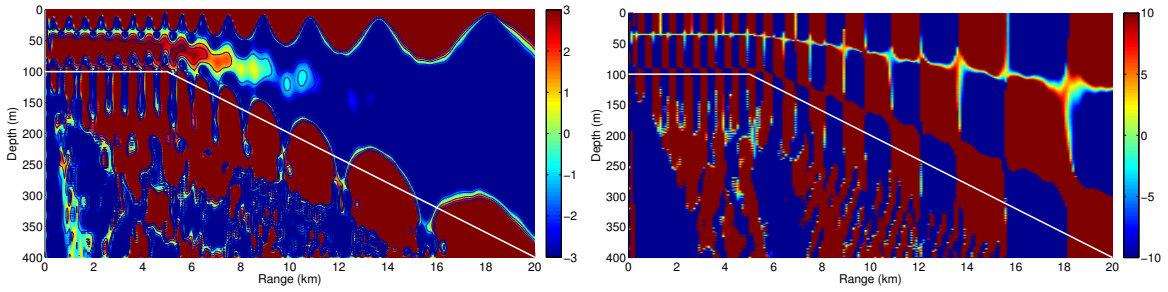

(a) Magnitude Error

(b) Phase Error

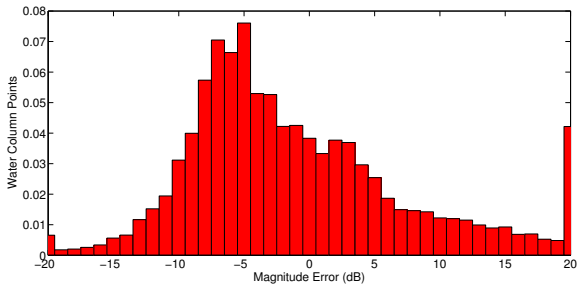

(c) Magnitude Error Distribution

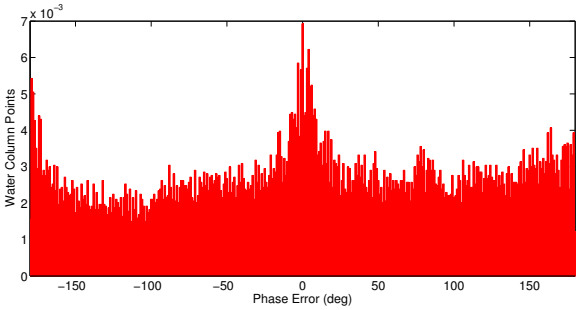

(d) Phase Error Distribution

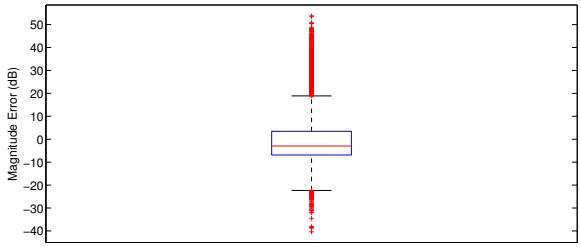

(e) Magnitude Error Statistics

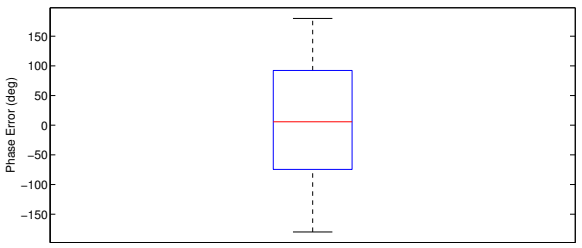

(f) Phase Error Statistics

Figure 2.10. Computational error calculating the received vertical velocity field in the shelf break environment using MMPE and scalar reciprocity. Magnitude error contours are drawn for ±1, ±2, and ±3 dB.

CHAPTER 3:
Vector-Scalar Reciprocity Equation Derivation and Applications

This derivation follows the general approach of Case [8] using the methods in [9]. All signals have an implied time dependence of $e^{-j\omega t}$ that is suppressed for brevity. Bold face indicates vector quantities.

3.1 Reciprocity for General Sources

The general form of the linearized inhomogeneous wave equation is [10]

$$\rho(\mathbf{r})\left[\nabla\cdot\frac{\nabla p_1(\mathbf{r})}{\rho(\mathbf{r})}\right]+k^2p_1(\mathbf{r})=j\omega M_1(\mathbf{r}-\mathbf{r_1})+\nabla\cdot\mathbf{F_1}(\mathbf{r}-\mathbf{r_1}) \tag{3.1}$$

where $p_1(\mathbf{r})$ is the pressure at $\mathbf{r}$ given a source at $\mathbf{r_1}$ that is a superposition of two different types of sources. The first source is an acoustic monopole that produces mass injection rate per unit volume M_1. The second source is an acoustic dipole that produces directional force per unit volume $\mathbf{F_1}$. Now consider two solutions to Equation (3.1): $p_1(\mathbf{r})$ for a source at $\mathbf{r_1}$ and $p_2(\mathbf{r})$ for a source at $\mathbf{r_2}$. Multiply the first equation by p_2, and multiply the second equation by p_1; then subtract the second equation from the first and integrate over the volume of interest,

$$\begin{aligned}&\int_V\left[p_2(\mathbf{r})\nabla\cdot\frac{\nabla p_1(\mathbf{r})}{\rho(\mathbf{r})}-p_1(\mathbf{r})\nabla\cdot\frac{\nabla p_2(\mathbf{r})}{\rho(\mathbf{r})}\right]dV\\&=\int_V\left[\frac{p_2(\mathbf{r})}{\rho(\mathbf{r})}j\omega M_1(\mathbf{r}-\mathbf{r_1})+\frac{p_2(\mathbf{r})}{\rho(\mathbf{r})}\nabla\cdot\mathbf{F_1}(\mathbf{r}-\mathbf{r_1})\right]dV\\&-\int_V\left[\frac{p_1(\mathbf{r})}{\rho(\mathbf{r})}j\omega M_2(\mathbf{r}-\mathbf{r_2})+\frac{p_1(\mathbf{r})}{\rho(\mathbf{r})}\nabla\cdot\mathbf{F_2}(\mathbf{r}-\mathbf{r_2})\right]dV.\end{aligned} \tag{3.2}$$

Applying Green's Theorem to the left hand side of Equation (3.2) converts it to a surface integral that vanishes for the impedance boundary conditions one encounters in underwater acoustics since potentials are proportional to their gradients. Therefore, the integrals on the right hand side must be equal.

This is the form of the general reciprocity relationship for pressure and velocity,

$$\int_V \left[\frac{p_2(\mathbf{r})}{\rho(\mathbf{r})} j\omega M_1(\mathbf{r}-\mathbf{r_1}) + \frac{p_2(\mathbf{r})}{\rho(\mathbf{r})} \nabla \cdot \mathbf{F_1}(\mathbf{r}-\mathbf{r_1}) \right] dV = \int_V \left[\frac{p_1(\mathbf{r})}{\rho(\mathbf{r})} j\omega M_2(\mathbf{r}-\mathbf{r_2}) + \frac{p_1(\mathbf{r})}{\rho(\mathbf{r})} \nabla \cdot \mathbf{F_2}(\mathbf{r}-\mathbf{r_2}) \right] dV. \quad (3.3)$$

3.2 Reciprocity for Point Sources

Equation (3.3) can be further simplified for point sources. Let each monopole source take the form $M(\mathbf{r}-\mathbf{r_1}) = M_1\delta(\mathbf{r}-\mathbf{r_1})$, and let each dipole source take the form $\mathbf{F}(\mathbf{r}-\mathbf{r_1}) = \mathbf{F_1}\delta(\mathbf{r}-\mathbf{r_1})$ where $\delta(\cdot)$ is the three dimensional Dirac delta function. Then the ∇ operator can be changed from $\mathbf{F}$ to p via integration by parts and the Divergence Theorem, i.e.,

$$\begin{aligned} \int_V g\,(\nabla \cdot \mathbf{A})\,dV &= -\int_V \mathbf{A} \cdot (\nabla g)\,dV + \int_V \nabla \cdot (g\mathbf{A})\,dV \\ &= -\int_V \mathbf{A} \cdot (\nabla g)\,dV + \oint_S (g\mathbf{A})\,dS. \end{aligned}$$

When $g = p_2(\mathbf{r})/\rho(\mathbf{r})$ and $\mathbf{A} = \mathbf{F_1}\delta(\mathbf{r}-\mathbf{r_1})$, the surface integral vanishes since the delta function is zero everywhere on the surface, and the volume integral becomes the dot product of the force and the gradient of the pressure. Equation (3.3) can now be rewritten as

$$\int_V \left[\frac{j\omega M_1 \delta(\mathbf{r}-\mathbf{r_1})}{\rho(\mathbf{r})} p_2(\mathbf{r}) - \mathbf{F_1}\delta(\mathbf{r}-\mathbf{r_1}) \cdot \nabla \left(\frac{p_2(\mathbf{r})}{\rho(\mathbf{r})} \right) \right] dV = \int_V \left[\frac{j\omega M_2 \delta(\mathbf{r}-\mathbf{r_2})}{\rho(\mathbf{r})} p_1(\mathbf{r}) - \mathbf{F_2}\delta(\mathbf{r}-\mathbf{r_2}) \cdot \nabla \left(\frac{p_1(\mathbf{r})}{\rho(\mathbf{r})} \right) \right] dV. \quad (3.4)$$

Integration over the entire volume extracts only those values where the delta functions are nonzero at the source locations $\mathbf{r_1}$ and $\mathbf{r_2}$, resulting in

$$\frac{j\omega M_1 p_2(\mathbf{r_1})}{\rho(\mathbf{r_1})} - \mathbf{F_1} \cdot \nabla \left(\frac{p_2(\mathbf{r_1})}{\rho(\mathbf{r_1})} \right) = \frac{j\omega M_2 p_1(\mathbf{r_2})}{\rho(\mathbf{r_2})} - \mathbf{F_2} \cdot \nabla \left(\frac{p_1(\mathbf{r_2})}{\rho(\mathbf{r_2})} \right). \quad (3.5)$$

The gradient terms in this equation can be rewritten as

$$\nabla\left(\frac{p(\mathbf{r})}{\rho(\mathbf{r})}\right) = \nabla\left(\frac{p(\mathbf{r})}{\rho_0(1+s(\mathbf{r}))}\right), \tag{3.6}$$

where ρ_0 is the constant equilibrium density and $s(\mathbf{r})$ is the condensation. In [10] the derivation of the wave equation used in Equation (3.1) required a linearization of the equation of continuity and Euler's equation. In both of these linearizations, there was an assumption that $s(\mathbf{r}) \ll 1$. In many cases, such as in the water column or in a homogeneous layer, that assumption is still valid, so the gradient term can be reduced to

$$\nabla\left(\frac{p(\mathbf{r})}{\rho(\mathbf{r})}\right) = \frac{\nabla p(\mathbf{r})}{\rho_0} = j\omega\mathbf{v}(\mathbf{r}), \tag{3.7}$$

since $\nabla p(\mathbf{r}) = j\omega\rho_0\mathbf{v}(\mathbf{r})$. There are situations where this assumption does not hold, such as at boundaries between layers or in an inhomogeneous layer, because the density gradient is not exactly zero. In these cases the full gradient term must be evaluated

$$\nabla\left(\frac{p(\mathbf{r})}{\rho(\mathbf{r})}\right) = \frac{\nabla p(\mathbf{r})}{\rho(\mathbf{r})} + \nabla\left(\frac{1}{\rho(\mathbf{r})}\right)p(\mathbf{r}). \tag{3.8}$$

Nevertheless, returning to the common case where the condensation is small throughout the water column, the reciprocity relationship for point sources can be stated with both a pressure component and a velocity component as

$$M_1\frac{p_2(\mathbf{r_1})}{\rho(\mathbf{r_1})} - \mathbf{F_1}\cdot\mathbf{v_2}(\mathbf{r_1}) = M_2\frac{p_1(\mathbf{r_2})}{\rho(\mathbf{r_2})} - \mathbf{F_2}\cdot\mathbf{v_1}(\mathbf{r_2}). \tag{3.9}$$

3.3 Applications

The point source reciprocity relationship has different applications depending on the choice of sources used. Two monopole sources relate pressure to pressure, two dipole sources relate velocity to velocity, and a mix of monopole and dipole sources relates pressure to velocity.

3.3.1 Scalar Reciprocity

When only monopole sources of equal amplitude are considered, then $M_1 = M_2$ and $\mathbf{F_1} = \mathbf{F_2} = 0$, and Equation (3.9) reduces to

$$\frac{p_2(\mathbf{r_1})}{\rho(\mathbf{r_1})} = \frac{p_1(\mathbf{r_2})}{\rho(\mathbf{r_2})}. \tag{3.10}$$

This is the familiar form found in Equation (1.1), [1], and [9] equating the pressure at point 2 due to a source at point 1 to the pressure at point 1 due to a source at point 2.

3.3.2 Vector Reciprocity

Similarly, when only dipole sources are considered, $M_1 = M_2 = 0$, and Equation (3.9) becomes

$$\mathbf{F_1} \cdot \mathbf{v_2}(\mathbf{r_1}) = \mathbf{F_2} \cdot \mathbf{v_1}(\mathbf{r_2}). \tag{3.11}$$

This is the reciprocal relationship between velocity and force components. When Equation (3.11) is expanded in Cartesian coordinates it becomes

$$F_{1x}v_{2x}(\mathbf{r_1}) + F_{1y}v_{2y}(\mathbf{r_1}) + F_{1z}v_{2z}(\mathbf{r_1}) = F_{2x}v_{1x}(\mathbf{r_2}) + F_{2y}v_{1y}(\mathbf{r_2}) + F_{2z}v_{1z}(\mathbf{r_2}). \tag{3.12}$$

This equation is easier to use when the forces are restricted to a single axis. For example, when both forces act only in the x direction, Equation (3.12) reduces to

$$F_{1x}v_{2x}(\mathbf{r_1}) = F_{2x}v_{1x}(\mathbf{r_2}). \tag{3.13}$$

When the amplitudes of the force components are equal, $F_{1x} = F_{2x}$, and Equation (3.13) states that the x velocity received at point 2 due to a force in the x direction at point 1 is equal to the x velocity received at point 1 due to a force in the x direction at point 2. The same applies to two forces in the y direction and two forces in the z direction.

Equation (3.12) has a less obvious application when the two forces act in orthogonal directions. For example, when the first force acts in the x direction and the second force acts in the y direction, Equation (3.12) becomes

$$F_{1x}v_{2x}(\mathbf{r_1}) = F_{2y}v_{1y}(\mathbf{r_2}). \tag{3.14}$$

When the force components are equal, $F_{1x} = F_{2y}$, and Equation (3.14) states that the y velocity received at point 2 due to a force in the x direction at point 1 is equal to the x velocity received at point 1 due to a force in the y direction at point 2. This relationship holds for all six pairs of forces in orthogonal directions.

Equation (3.11) is useful for calculating the received velocity components at a fixed location due to a dipole source at any range and depth in the environment. Suppose the dipole source is oriented along the x axis. First compute the x velocity everywhere in the field for a point force with unit amplitude at the desired receiver location oriented in the x direction. This quantity is represented by $v_x^{(X)}$, where the subscript x represents the field component that is calculated, and the superscript (X) represents the source orientation used to calculate it. By vector reciprocity, this is equal to the x velocity received at the desired fixed position for a force in the x direction at any source location in the field. Next place a force at the desired receiver location but orient it in the y direction. Calculate the x velocity everywhere in the field, $v_x^{(Y)}$. This is equal to the y velocity received at the desired fixed position for a force in the x direction at any source location in the field. Finally, place a force at the receiver location oriented along the z axis. Calculate the x velocity everywhere in the field, $v_x^{(Z)}$. This is equal to the z velocity received at the desired fixed position for a force in the x direction at any source location in the field. Finally, since the fields were calculated with a unit amplitude source, multiply each quantity by the dipole source amplitude F_x.

Since any force can be decomposed into a sum of components in each orthogonal direction, this process can be extended to arbitrary source orientations via superposition. The reciprocal velocity field must be calculated for each orthogonal source direction. This can be accomplished with three propagation model runs provided all three velocity components are saved for each model run, e.g. $v_x^{(X)}$, $v_y^{(X)}$, and $v_z^{(X)}$ for the source in the x direction. This produces three x velocities ($v_x^{(X)}$, $v_x^{(Y)}$, $v_x^{(Z)}$), three y velocities ($v_y^{(X)}$, $v_y^{(Y)}$, $v_y^{(Z)}$), and three z velocities ($v_z^{(X)}$, $v_z^{(Y)}$, $v_z^{(Z)}$). The total x velocity is the inner product of the three x velocities with the three force components, the total y velocity is the inner product of the three y velocities with the three force components, and the total z velocity is the inner

product of the three z velocities with the three force components, i.e.,

$$\begin{aligned} v_x &= F_x v_x^{(X)} + F_y v_x^{(Y)} + F_z v_x^{(Z)} \\ v_y &= F_x v_y^{(X)} + F_y v_y^{(Y)} + F_z v_y^{(Z)} \\ v_z &= F_x v_z^{(X)} + F_y v_z^{(Y)} + F_z v_z^{(Z)}. \end{aligned} \tag{3.15}$$

3.3.3 Vector-Scalar Reciprocity

The final reciprocal relationship arises when $M_1 = 0$ and $\mathbf{F_2} = 0$. This reduces Equation (3.9) to

$$-\mathbf{F_1} \cdot \mathbf{v_2}(\mathbf{r_1}) = M_2 \frac{p_1(\mathbf{r_2})}{\rho(\mathbf{r_2})}. \tag{3.16}$$

This form of the reciprocity relationship for point sources permits the computational shortcut commonly used for received pressure calculations to be used for received velocity calculations. Normally, a monopole source is placed in the desired receiver location and the acoustic field is calculated everywhere for that source. This pressure is then scaled by the density ratio of source and receiver locations. By reciprocity, this quantity is the pressure received at that desired fixed position for a source located at each point in the field.

Applying this method to Equation (3.16) is a two-step process. First, a dipole source is placed in a particular orientation (aligned with the x, y, or z axis) at the desired receiver location and the pressure field is calculated everywhere for that source. The pressure at each point in the field is then divided by the density and negated to account for the direction reversal. Provided the sources have equivalent magnitudes, $|M_2| = \|\mathbf{F_1}\|$, the result is the amplitude of the velocity component in the same direction that the dipole was oriented in the first step. To obtain the other received velocity components, these steps are repeated for other orientations of a source dipole at the desired receiver location.

3.3.4 Inverse Vector Fields

When combined with a propagation model that calculates pressure and velocity components of the vector field for a fixed source, Equations (3.10), (3.11), and (3.16) enable the reciprocal computation of the vector field for a fixed receiver from the solution to a monopole or dipole source. Let the model calculate the received pressure, radial velocity, and vertical velocity

for a monopole source at the fixed receiver location, $p^{(M)}$, $v_r^{(M)}$, and $v_z^{(M)}$. Likewise, the model outputs for a horizontal dipole source are $p^{(H)}$, $v_r^{(H)}$, and $v_z^{(H)}$, and the model outputs for a vertical dipole source are $p^{(V)}$, $v_r^{(V)}$, and $v_z^{(V)}$. Using these model outputs properly scaled for units of Pascals and meters per second, the received pressure and velocity for a fixed receiver and monopole source are

$$\begin{aligned} p &= p^{(M)} \\ v_r &= \left(\frac{1}{\rho_0 c}\right) p^{(H)} \\ v_z &= \left(\frac{1}{\rho_0 c}\right) p^{(V)}, \end{aligned} \tag{3.17}$$

the received pressure and velocity for a fixed receiver and horizontal dipole source are

$$\begin{aligned} p &= (\rho_0 c)\, v_r^{(M)} \\ v_r &= v_r^{(H)} \\ v_z &= v_r^{(V)}, \end{aligned} \tag{3.18}$$

and the received pressure and velocity for a fixed receiver and vertical dipole source are

$$\begin{aligned} p &= (\rho_0 c)\, v_z^{(M)} \\ v_r &= v_z^{(H)} \\ v_z &= v_z^{(V)}. \end{aligned} \tag{3.19}$$

A dipole with arbitrary orientation within the plane of calculation can be parameterized by its rotation from vertical by an angle φ. For a unit magnitude source, the horizontal and vertical components of this dipole are equal to $\sin(\varphi)$ and $\cos(\varphi)$, respectively. The received pressure and velocity for a fixed receiver and arbitrarily-rotated source are

$$\begin{aligned} p &= (\rho_0 c)\, v_r^{(M)} \sin(\varphi) + (\rho_0 c)\, v_z^{(M)} \cos(\varphi) \\ v_r &= v_r^{(H)} \sin(\varphi) + v_z^{(H)} \cos(\varphi) \\ v_z &= v_r^{(V)} \sin(\varphi) + v_z^{(V)} \cos(\varphi), \end{aligned} \tag{3.20}$$

of which the horizontal and vertical dipole are special cases for $\varphi = \frac{\pi}{2}$ and $\varphi = 0$. These results are for a model that calculates field components in a single plane with one vertical axis z and one horizontal axis r, but it immediately extends to a model that calculates a full three-dimensional field. In that case a dipole source can also be arbitrarily rotated by an angle ϑ in the horizontal plane, so the full direction cosines needed to combine model outputs are $\cos(\vartheta)\sin(\varphi)$, $\sin(\vartheta)\sin(\varphi)$, and $\cos(\varphi)$.

CHAPTER 4:
Demonstration of the Vector-Scalar Reciprocity Equation

The vector-scalar reciprocity relationship in Equation (3.16) can be demonstrated analytically and numerically if it correctly calculates the received vector fields for the range-independent and range-dependent environments that the pressure reciprocity relationship failed to calculate in Chapter 2.

4.1 Analytic Expressions for Vector-Scalar Reciprocity in a Range-Independent Environment

This new reciprocity relationship can be applied to the range-independent environment from Section 2.1 by calculating analytic expressions for the pressure field created by horizontal and vertical dipoles. Haug et al. [11] developed an expression for the pressure generated by a dipole source by expanding the field around the source in a Taylor series. For a dipole of source strength $F_1 = \|\mathbf{F_1}\|$ at point $\mathbf{r_1}$ rotated φ from the vertical axis and ϑ from the radial axis in the horizontal plane, it produces

$$p(\mathbf{r_2}) = \frac{F_1}{4j}\sum_{m=0}^{\infty}\Big[-\Psi_m(z_2)\Psi_m(z_1)k_{rm}H_1^{(1)}(k_{rm}r)\sin(\varphi)\cos(\vartheta-\theta) + \Psi_m(z_2)\Psi_m'(z_1)H_0^{(1)}(k_{rm}r)\cos(\varphi)\Big]. \quad (4.1)$$

Here $r = |r_2 - r_1|$ is the absolute horizontal distance between the source and receiver, which is the same as the distance r in Equations (2.1–2.3). Equation (4.1) is valid for any mode shape $\Psi(z)$, but plugging in the mode shapes for the Pekeris waveguide gives

$$p(\mathbf{r_2}) = \frac{F_1}{4j}\sum_{m=0}^{\infty}\Big[-A_m^2\sin(k_{zm}z_2)\sin(k_{zm}z_1)k_{rm}H_1^{(1)}(k_{rm}r)\sin(\varphi)\cos(\vartheta-\theta) + A_m^2\sin(k_{zm}z_2)k_{zm}\cos(k_{zm}z_1)H_0^{(1)}(k_{rm}r)\cos(\varphi)\Big]. \quad (4.2)$$

When the dipole is oriented horizontally, $\sin(\varphi) = 1$ and $\cos(\varphi) = 0$, so the first bracketed term in Equation (4.2) determines the pressure. When the dipole is then aligned with the plane in which the field components are to be calculated, $\cos(\vartheta - \theta) = 1$, and the pressure is

$$p(\mathbf{r_2}) = \frac{-F_1}{4j} \sum_{m=0}^{\infty} A_m^2 \sin(k_{zm} z_2) \sin(k_{zm} z_1) k_{rm} H_1^{(1)}(k_{rm} r). \tag{4.3}$$

Similarly, when the source dipole is oriented vertically, $\cos(\varphi) = 1$ and $\sin(\varphi) = 0$, so the pressure field is determined entirely by the second bracketed term in Equation (4.2),

$$p(\mathbf{r_2}) = \frac{F_1}{4j} \sum_{m=0}^{\infty} A_m^2 \sin(k_{zm} z_2) k_{zm} \cos(k_{zm} z_1) H_0^{(1)}(k_{rm} r). \tag{4.4}$$

When the source is scaled according to the vector-scalar reciprocity relationship, $F_1 = -M_2/\rho_0 = -1/\rho_0$, and the pressure is converted to velocity through division by $j\omega\rho_0$, these are exactly equal to the velocity expressions in Equations (2.8) and (2.9). Therefore, the quantity in the brackets in Equation (4.2) is the dot product of the dipole source with the received velocity due to a monopole source, as predicted in Equation (3.16).

4.2 Numerical Solutions to the Range-Independent Environment

Pressure reciprocity was already demonstrated using a monopole source at the receiver location. Now the reciprocal field for radial velocity is calculated with MMPE using a horizontal dipole source at the receiver location, and the reciprocal field for vertical velocity is calculated with MMPE using a vertical dipole source. The method used to modify MMPE to create fields for dipole sources rather than its standard monopole source is described in the appendix. Since the received field to be calculated here is for a monopole source, the reciprocal velocity fields are the MMPE pressure output for each of the directional sources divided by the characteristic acoustic impedance.

Figure 4.1 shows the vector field components measured by a fixed receiver for the range-independent Pekeris waveguide using the vector reciprocity relationship. The radial velocity field is once again in good agreement with the reference solution. This is borne out by the error analysis in Figure 4.2. The magnitude error for radial velocity has a mean of

1.31% and a standard deviation of 9.67%. The phase error has mean -0.648 degrees and standard deviation 4.71 degrees. These numbers are comparable to the statistics for the reciprocal radial velocity calculated with a monopole source in Section 2.2, but that is what the equations predicted for a range-independent environment.

As compared to Figure 2.2, the reciprocal vertical velocity field in the left column is a much closer match to the reference field in the right column. Figure 4.3 shows how little error

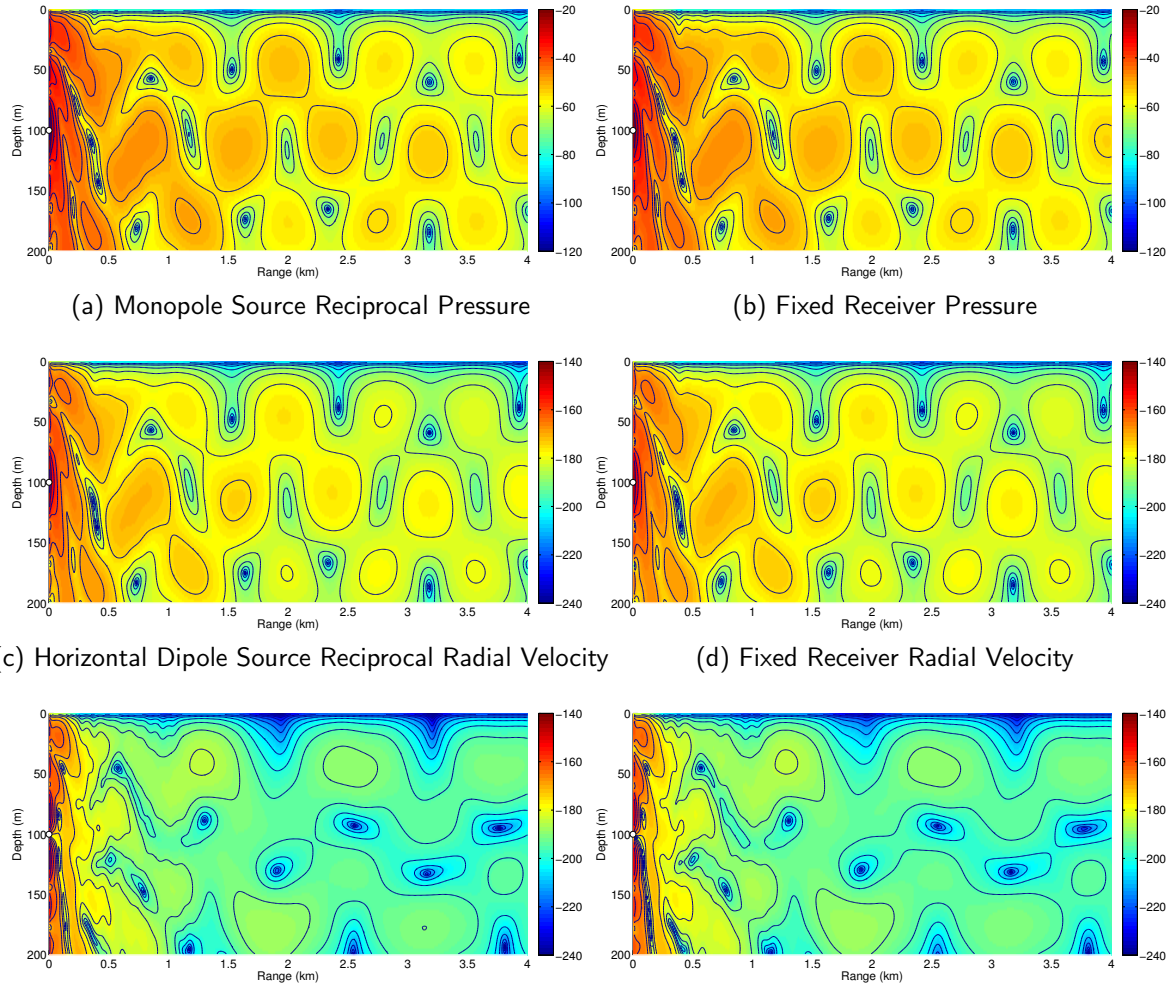

(a) Monopole Source Reciprocal Pressure

(b) Fixed Receiver Pressure

(c) Horizontal Dipole Source Reciprocal Radial Velocity

(d) Fixed Receiver Radial Velocity

(e) Vertical Dipole Source Reciprocal Vertical Velocity

(f) Fixed Receiver Vertical Velocity

Figure 4.1. Vector field components in the Pekeris waveguide calculated with MMPE using scalar and vector-scalar reciprocity. Pressure is in dB//1Pa. Velocity is in dB//1m/s. Transmission loss contours are drawn every 5 dB.

there is between solutions. The vertical velocity magnitude error mean is much lower at 0.755%, but more importantly, the standard deviation has reduced from 945% to 14.0%. Similarly, the phase error mean is -0.398 degrees and the standard deviation has reduced from 99.6 degrees to 5.42 degrees. For the first kilometer of range, there is slightly more variation in the vertical velocity reciprocal field with many small regions of fluctuation. Beyond one kilometer, the vertical velocity field settles into its far-field pattern and the errors are restricted to locations of nulls in the field due to destructive interference.

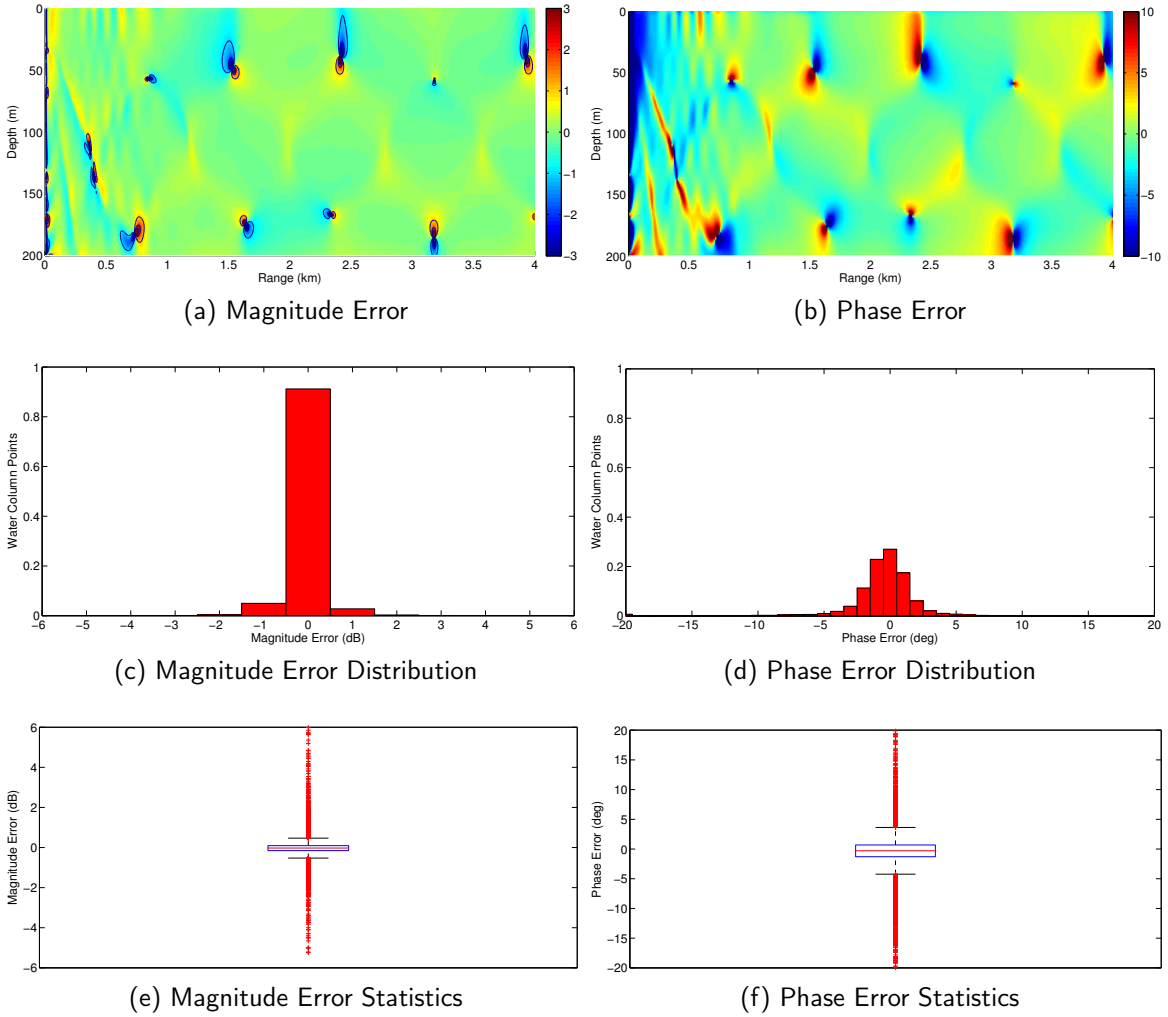

(a) Magnitude Error

(b) Phase Error

(c) Magnitude Error Distribution

(d) Phase Error Distribution

(e) Magnitude Error Statistics

(f) Phase Error Statistics

Figure 4.2. Computational error calculating the received radial velocity field in the Pekeris waveguide using MMPE and vector-scalar reciprocity. Magnitude error contours are drawn for ±1, ±2, and ±3 dB.

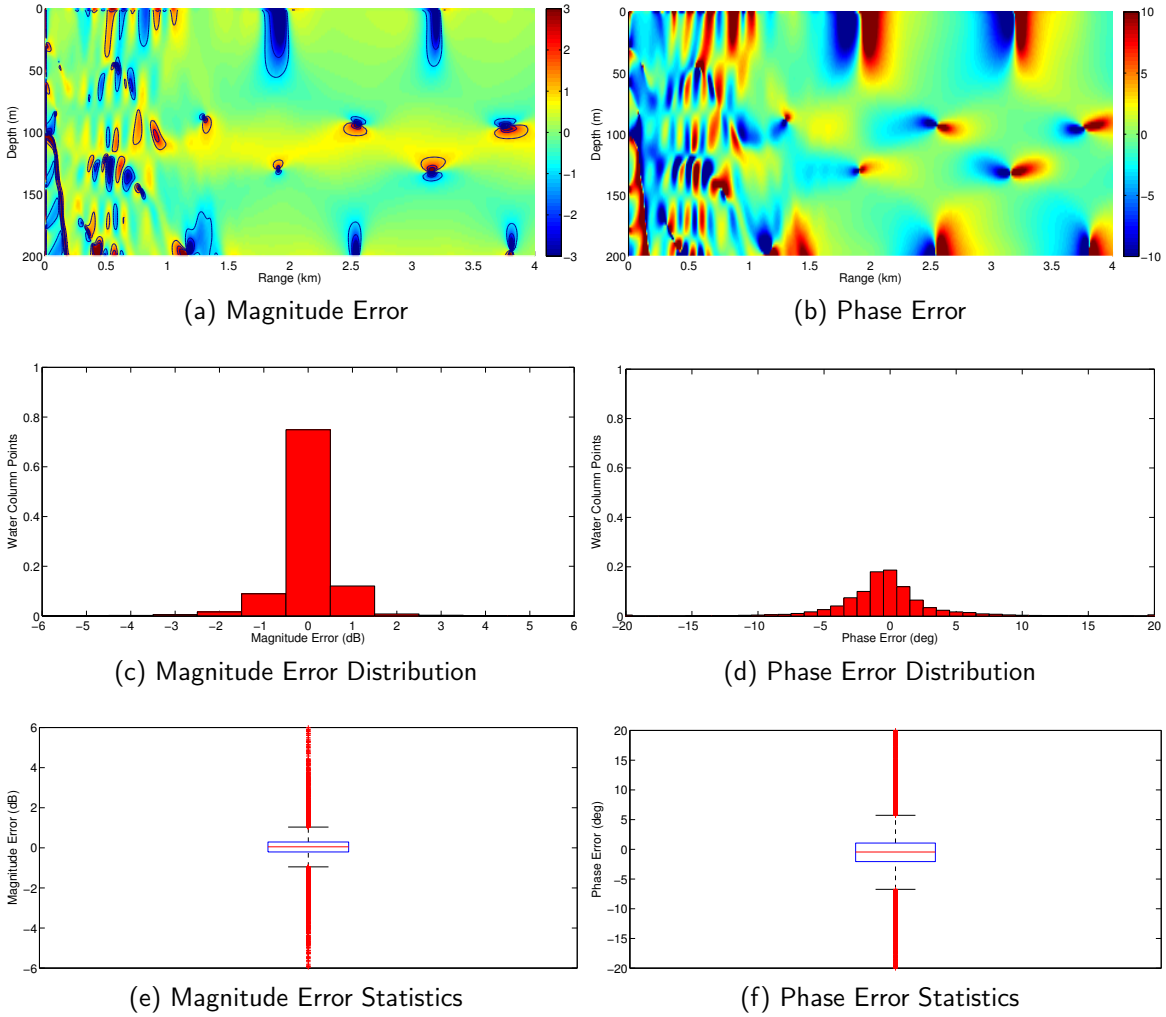

(a) Magnitude Error

(b) Phase Error

(c) Magnitude Error Distribution

(d) Phase Error Distribution

(e) Magnitude Error Statistics

(f) Phase Error Statistics

Figure 4.3. Computational error calculating the received vertical velocity field in the Pekeris waveguide using MMPE and vector-scalar reciprocity. Magnitude error contours are drawn for ±1, ±2, and ±3 dB.

Table 4.1 lists the summary statistics for error in calculating the received vector field using the vector reciprocity principle. The improvement in vertical velocity calculation method is evident when this table is compared to Table 2.2.

Table 4.1. Vector field calculation error statistics using scalar and vector-scalar reciprocity for a monopole source in a Pekeris waveguide

		Pressure	Radial Velocity	Vertical Velocity
Magnitude (%)	mean	0.618	1.31	0.733
	std	10.0	9.67	14.0
Phase (deg)	mean	-0.0501	-0.648	-0.398
	std	3.28	4.71	5.42

These results come at a substantial computational savings. Generating the reference field with 2-meter depth resolution and 10-meter range resolution required 40,100 model runs to calculate the received pressure, radial velocity, and vertical velocity to a maximum range of 4 km. In contrast, the same resolution was achieved in 3 model runs using the scalar and vector-scalar reciprocity methods.

4.3 Numerical Solutions to the Range-Dependent Environment

Returning to the range-dependent environment from Section 2.3, the baseline reference fields for model comparison are from the same set of MMPE runs with a monopole source at depth intervals of 2 m and range intervals of 100 m. The reciprocal pressure is calculated as before with a monopole source, but the reciprocal vector fields are now calculated using horizontal and vertical dipole sources. The resulting fields are shown in Figure 4.4.

Calculating the received radial velocity field using the reciprocity relationship for a horizontal dipole source produces an excellent match to the reference field, as shown in Figure 4.5. Unlike the incorrect method shown in Figure 2.9, the magnitude and phase errors do not grow in range but remain relatively constant. For all field points in the water column, the magnitude error mean is 0.577%, and the standard deviation is 29.2%. The phase error mean is -0.187 degrees, and the standard deviation is 10.6 degrees. These statistics are comparable to the statistics for the reciprocal pressure calculation error in Section 2.3.

Even more pronounced than the improvement in reciprocal calculation for the radial velocity field is the improvement in the reciprocal vertical velocity field calculated with a vertical dipole source at the receiver location. This is demonstrated in Figure 4.6. In stark contrast to the incorrect reciprocal method shown in Figure 2.10, this method produces a close match to the reference solution for both magnitude and phase. The magnitude error mean and standard deviation for all field points in the water column are 5.44% and 53.1%, and the phase error mean and standard deviation for all field points are -0.505 degrees and 10.0 degrees. As with the radial velocity, these error statistics are comparable to the reciprocal pressure error statistics.

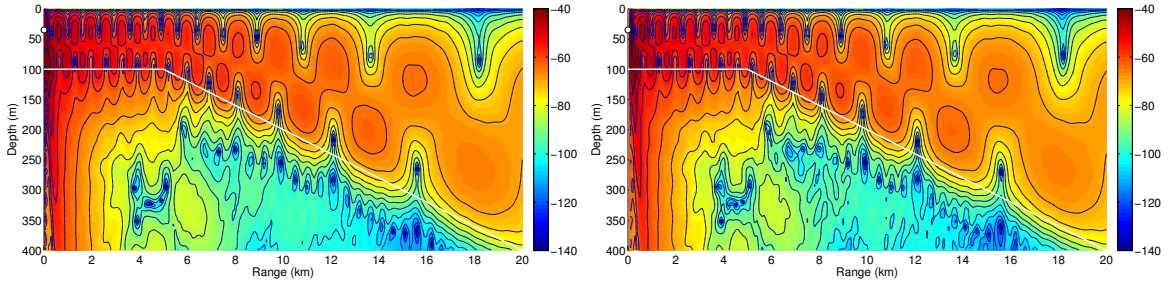

(a) Monopole Source Reciprocal Pressure

(b) Fixed Receiver Pressure

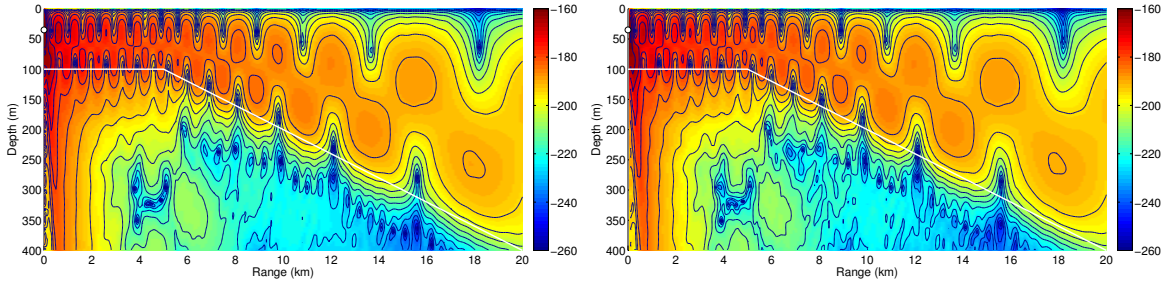

(c) Horizontal Dipole Source Reciprocal Radial Velocity

(d) Fixed Receiver Radial Velocity

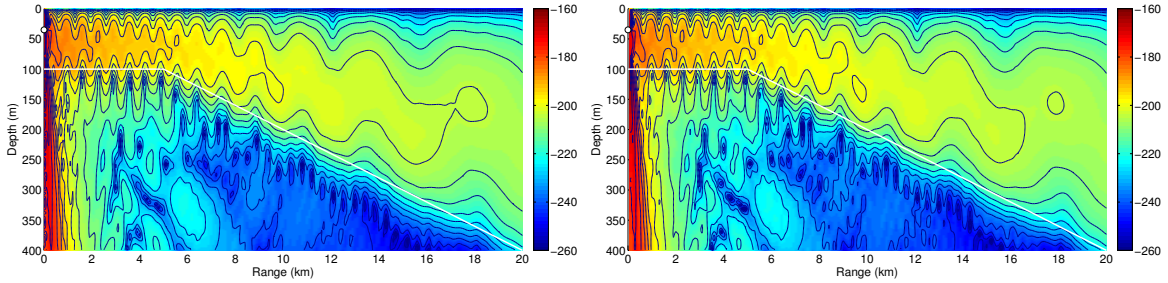

(e) Vertical Dipole Source Reciprocal Vertical Velocity

(f) Fixed Receiver Vertical Velocity

Figure 4.4. Vector field components in the shelf break environment calculated with MMPE using scalar and vector-scalar reciprocity. Pressure is in dB//1Pa. Velocity is in dB//1m/s. Transmission loss contours are drawn every 5 dB.

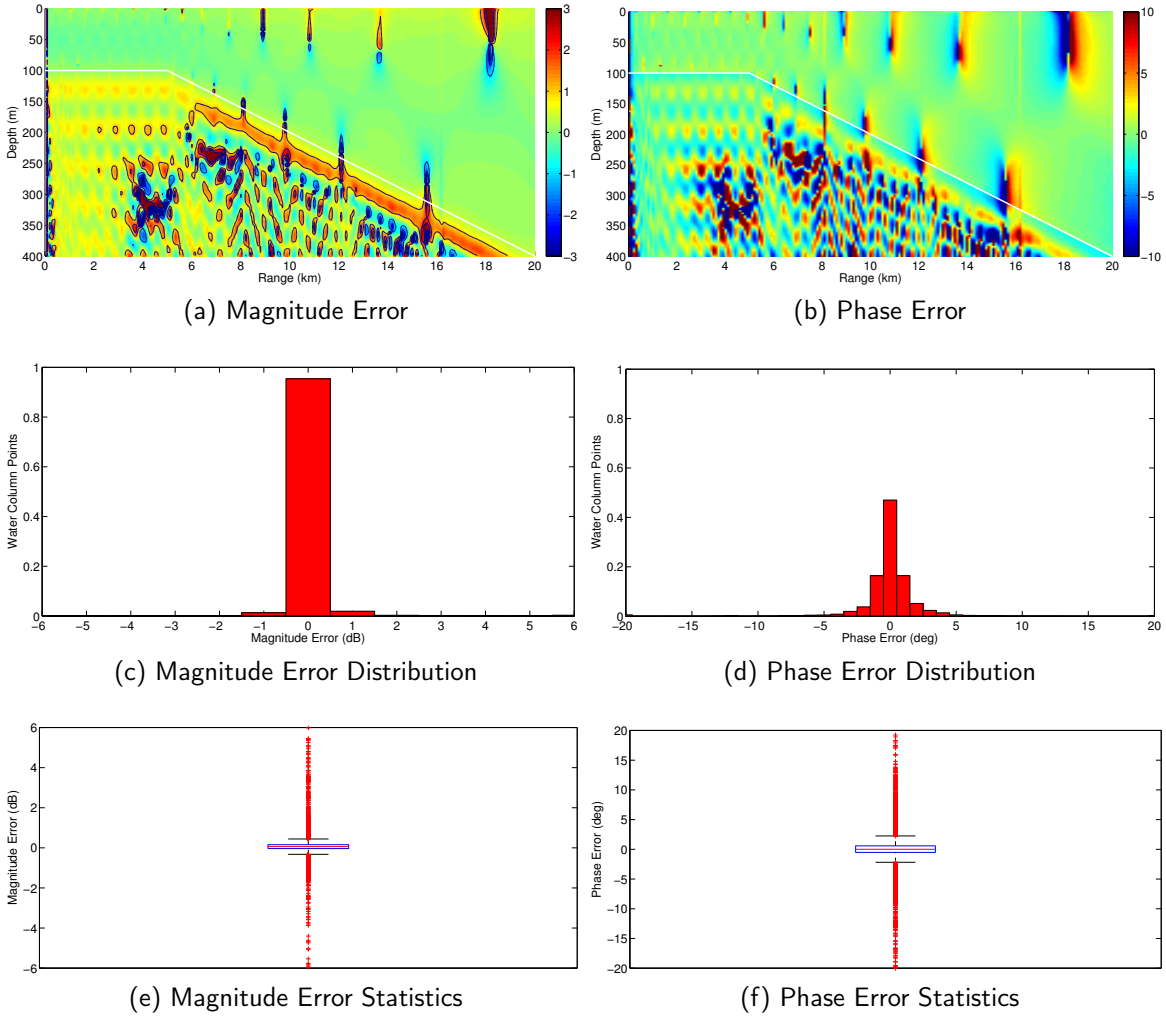

(a) Magnitude Error

(b) Phase Error

(c) Magnitude Error Distribution

(d) Phase Error Distribution

(e) Magnitude Error Statistics

(f) Phase Error Statistics

Figure 4.5. Computational error calculating the received radial velocity field in the shelf break environment using MMPE and vector-scalar reciprocity. Magnitude error contours are drawn for ±1, ±2, and ±3 dB.

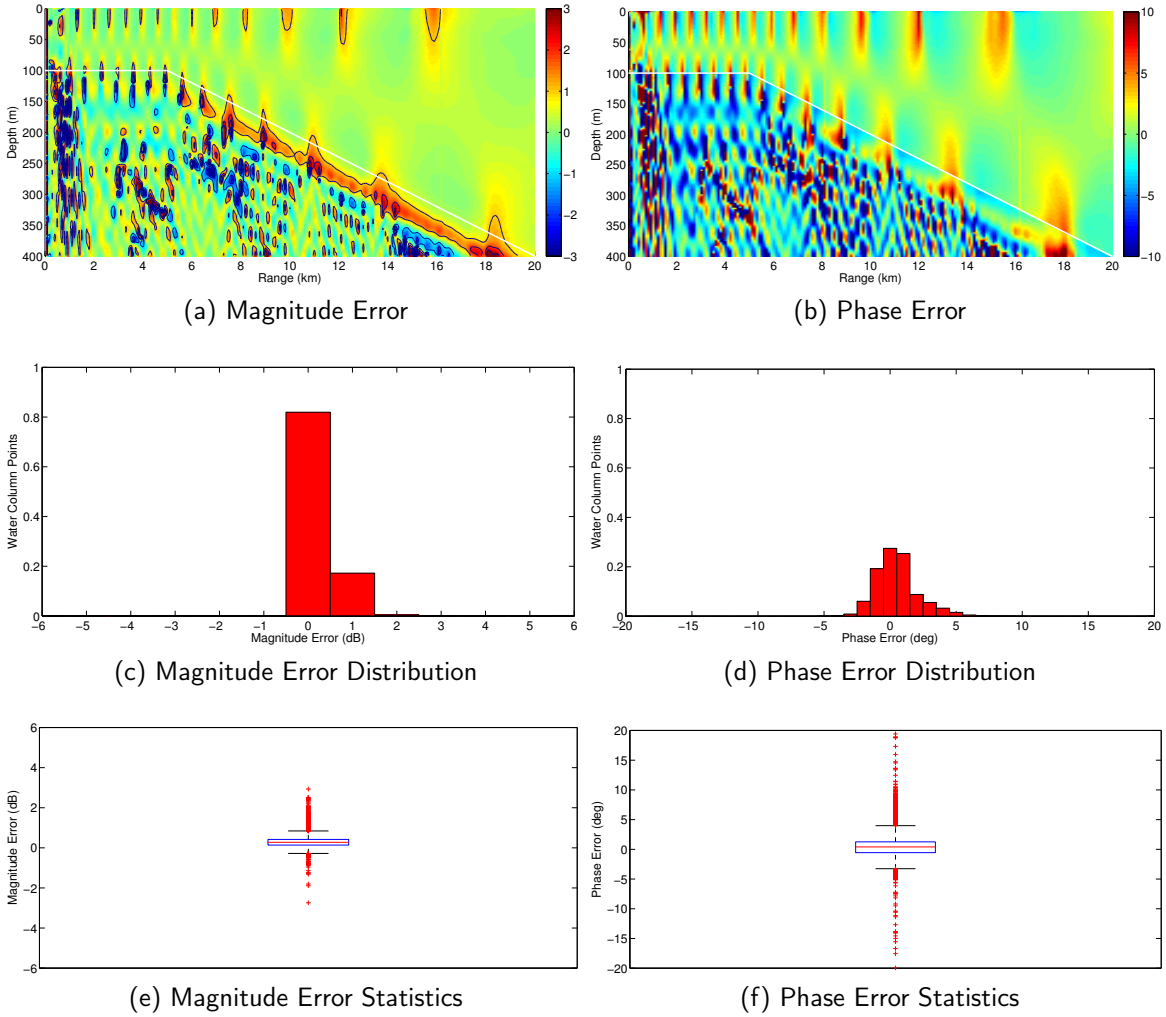

(a) Magnitude Error

(b) Phase Error

(c) Magnitude Error Distribution

(d) Phase Error Distribution

(e) Magnitude Error Statistics

(f) Phase Error Statistics

Figure 4.6. Computational error calculating the received vertical velocity field in the shelf break environment using MMPE and vector-scalar reciprocity. Magnitude error contours are drawn for ±1, ±2, and ±3 dB.

The statistics for the reciprocal vector field calculation for a monopole source at all locations in the water column of the shelf break range-dependent environment are summarized in Table 4.2. These results demonstrate that the vector-scalar reciprocity relationship is valid in arbitrary, range-dependent environments, and it can be used by acoustic propagation models to generate accurate vector fields at a fraction of the computational expense required for calculating those fields point by point.

Table 4.2. Vector field calculation error statistics using scalar and vector-scalar reciprocity for a monopole source in the water column of the shelf break range-dependent environment

		Pressure	Radial Velocity	Vertical Velocity
Magnitude (%)	mean	1.85	0.577	5.44
	std	31.1	29.2	53.1
Phase (deg)	mean	-0.0579	-0.235	0.543
	std	7.78	8.09	3.03

Once again, the vector-scalar reciprocity method provided a significant computational savings. The reference fields for the shelf break environment required 40,200 model runs to achieve 2-meter depth resolution and 100-meter range resolution. The scalar and vector-scalar reciprocity methods calculated the same fields in 3 model runs with a 2-meter depth resolution and 10-meter range resolution. Achieving the same range resolution with the moving monopole source method would have required an additional 360,000 model runs.

THIS PAGE INTENTIONALLY LEFT BLANK

CHAPTER 5:
Conclusion

The fundamental inability of the classic scalar reciprocity equation to accurately predict vector fields stems from the assumptions in its derivation of monopole sources and receivers. When dipole sources are included in the reciprocity derivation, a more general form of the equation results. This equation correctly contains the scalar reciprocity relationship between monopole sources and pressure fields, the vector reciprocity relationship between dipole sources and vector fields, and the vector-scalar reciprocity relationship between monopole sources, dipole sources, scalar fields, and vector fields.

The scalar reciprocity equation and vector-scalar reciprocity equation were shown to accurately predict the received vector field created by a monopole source in a range-independent Pekeris waveguide and range-dependent shelf break environment. To accurately compute the reciprocal vector fields, the parabolic equation model MMPE was modified to produce vector field outputs for horizontal and vertical dipole sources.

The vector reciprocity equation relating vector fields to dipole sources was not demonstrated, but one application for it is predicting the received vector field created by wind-driven surface noise. This noise source is often represented by a large number of vertical dipoles evenly distributed on a horizontal layer less than a wavelength below the surface. Propagating the field from each source to a fixed receiver would be computationally intensive due to the large number of sources required, but by invoking the vector reciprocity principle, one propagation model run with a dipole source at the receiver location could predict the velocity received from the surface noise sources at all ranges.

The reciprocity equation derivation can also be repeated with higher order sources such as quadrupoles. Although like dipoles, quadrupoles tend to be inefficient radiators and are not commonly used in underwater acoustics, their inclusion in a reciprocal equation could provide some mathematical efficiency for calculating other quantities of interest such as field circularity or higher-order moments. When the proper relationship between source type and received quantity is observed, these vector and vector-scalar reciprocity equations are as useful as the scalar reciprocity equation.

THIS PAGE INTENTIONALLY LEFT BLANK

APPENDIX: Dipole Starter Fields for Parabolic Equation Propagation Models

Acoustic propagation codes that use the parabolic approximation to the linearized wave equation are commonly implemented as one-way marching algorithms that require an initial condition, or starter field. One way to define a starter field is to calculate the analytic solution for a monopole point source and its image reflected by the pressure release surface and transform that to the wavenumber domain as [6]

$$\begin{aligned} \hat{\psi}_m(k_z) &= \alpha A_M \int_{-\infty}^{\infty} [\delta(z - z_s) - \delta(z + z_s)]\, e^{-jk_z z} dz \qquad \text{(A.1)} \\ &= -2j\alpha A_M \sin(k_z z_s), \qquad \text{(A.2)} \end{aligned}$$

where α is a normalization factor, A_M is the point source amplitude, z_s is the source depth, and k_z is the vertical wavenumber. By superposition, the starter field for multiple sources M arranged vertically at depths z_{si} is

$$\hat{\psi}_m(k_z) = -2j\alpha \sum_{i=0}^{M-1} A_i \sin(k_z z_{si}). \qquad \text{(A.3)}$$

In MMPE, the full starter field includes a wavenumber-space taper function (designed to improve phase accuracy at higher angles, consistent with the WKB approximation) and a phase function that accounts for grid spacing,

$$\hat{\psi}_m(k_z) = -2j\sqrt{\frac{jR_0}{2\pi k}} \sin(k_z z_s) \left(1 - \frac{k_z^2}{k^2}\right)^{\frac{1}{4}} e^{jk_z \frac{dz}{2}}, \qquad \text{(A.4)}$$

where the normalization term and source amplitude have been combined into the term with the square root. To take advantage of the vector reciprocity principle in MMPE, additional starter fields must be defined for vertical and horizontal dipoles. Vecherin et al. [12] prescribe an equivalent source method that decomposes vertical and horizontal dipole sources into vertical monopole arrays with element amplitude weights such that the array source strength is equal to that of a single monopole. Although these amplitude weights and element spacings can be implemented with MMPE's existing vertical array source, the

utility of dedicated horizontal and vertical dipole sources led to a direct implementation of the starter field in the vertical wavenumber domain such that the user need only specify the source depth and frequency.

A.1 Vertical Dipole Starter

A vertical dipole is a special case of a vertical array with two elements 180 degrees out of phase with each other and separated by a distance $2\Delta z$ much smaller than a wavelength ($k\Delta z \leq 0.1$). The desired shape of the acoustic field for this source is $\cos(\phi)$ for angles ϕ measured from the vertical axis. The acoustic dipole has a moment equal to

$$D(\phi) = -2jk\Delta z A_z \cos(\phi), \tag{A.5}$$

so to give this source the same amplitude as a monopole with constant moment $D(\phi) = A_M$, each element in the dipole array must have amplitude

$$A_z = \frac{jA_M}{2k\Delta z}. \tag{A.6}$$

The 180 degree phase shift is accomplished by shifting one element +90 degrees and shifting the other by -90 degrees with an additional multiplication of $\pm j$. For this two-element array, with weights $+jA_z$ at depth $[z_s + \Delta z]$ and $-jA_z$ at depth $[z_s - \Delta z]$, Equation (A.4) becomes

$$\hat{\psi}_v(k_z) = -2j\sqrt{\frac{jR_0}{2\pi k}}\left[jA_z \sin(k_z[z_s + \Delta z]) - jA_z \sin(k_z[z_s - \Delta z])\right]\left(1 - \frac{k_z^2}{k^2}\right)^{\frac{1}{4}} e^{jk_z\frac{dz}{2}} \tag{A.7}$$

When this equation replaces the MMPE monopole starter field, the model outputs pressure, radial velocity, and vertical velocity for a vertical dipole source.

A.2 Horizontal Dipole Starter

The horizontal dipole has a desired shape of $\sin(\phi)$, which Vecherin represents as a sum of cosines for angles close to $\pi/2$ using the Taylor series approximation,

$$\sin(\phi) \approx 1 - \frac{1}{2}\cos^2(\phi) - \frac{1}{8}\cos^4(\phi). \tag{A.8}$$

Narrow-angle parabolic equation codes require only the first two terms in Equation (A.8); wide-angle parabolic equation codes such as MMPE require all three. The terms in Equation (A.8) can be represented by arrays of 1, 3, and 5 elements vertically spaced by $2\Delta z$.

Just as a $\cos(\phi)$ directivity pattern can be represented by a superposition of two monopoles 180 degrees out of phase separated by a small distance, $\cos^2(\phi)$ can be represented by a superposition of two dipoles 180 degrees out of phase separated by a small distance. With appropriate spacing, two of the monopoles can occupy the same position and their amplitudes add, which means only three monopoles are required to represent $\cos^2(\phi)$, where the amplitude of the center monopole is double that of the others and 180 degrees out of phase. This process extends to higher order terms, and in general, the directivity pattern $\cos^n(\phi)$ can be represented with a vertical array of $n-1$ monopoles. The repeated summation of equal strength monopoles results in element weights that follow the binomial coefficients with alternating signs, i.e.,

$$A_k = \frac{(-1)^k n!}{k!(n-k)!}; k = 0 \ldots n, \tag{A.9}$$

where k is the zero-based array element index. As with the vertical dipole, the individual elements in this array must also be scaled by the amplitude $A_x^n = \left(\frac{jA_M}{2k\Delta z}\right)^n$ to produce an overall moment amplitude equal to the monopole moment A_M. This term comes directly from the Taylor series expansion. Table A.1 lists the element weights required to produce each $\cos^n(\phi)$ term in Equation (A.8) including both A_k and A_x^n scaling factors.

Table A.1. Positions and weights to implement $\cos^n(\phi)$ directivity

Depth	1	$\cos^2(\phi)$	$\cos^4(\phi)$
$z_s - 4\Delta z$			A_x^4
$z_s - 2\Delta z$		A_x^2	$-4A_x^4$
z_s	1	$-2A_x^2$	$6A_x^4$
$z_s + 2\Delta z$		A_x^2	$-4A_x^4$
$z_s + 4\Delta z$			A_x^4

To approximate the $\sin(\phi)$ directivity pattern, the weights for each element in the vertical array are added according to Equation (A.8). This results in a five-element array with the

weights A_{0-4} shown in Table A.2. As with the vertical dipole starter, this approximation holds for ($k\Delta z \leq 0.1$). When the source depth is close to a boundary in terms of a wavelength, this representation of the horizontal dipole as an extended vertical array can create problems as the outermost elements can cross the boundary. While adding additional terms to the Taylor series expansion for $\sin(\phi)$ reduces errors at higher propagation angles, it comes at the penalty of increasing the vertical array extent. Therefore the best choice for array size is five elements since this is the minimum number of elements required to meet the wide-angle requirements of MMPE.

Table A.2. Positions and weights to approximate horizontal dipole source with a vertical array of monopoles

Depth	$\approx \sin(\phi)$
$z_s - 4\Delta z$	$A_0 = -\frac{1}{8}A_x^4$
$z_s - 2\Delta z$	$A_1 = -\frac{1}{2}A_x^2 + \frac{1}{2}A_x^4$
z_s	$A_2 = 1 + A_x^2 - \frac{3}{4}A_x^4$
$z_s + 2\Delta z$	$A_3 = -\frac{1}{2}A_x^2 + \frac{1}{2}A_x^4$
$z_s + 4\Delta z$	$A_4 = -\frac{1}{8}A_x^4$

For implementation in MMPE, each of these array elements sums with its image source to produce the starter field

$$\begin{aligned}\hat{\psi}_h(k_z) \;=\; & -2j\sqrt{\frac{jR_0}{2\pi k}}\,\big[A_0\sin(k_z[z_s-4\Delta z]) \\ & +A_1\sin(k_z[z_s-2\Delta z]) + A_2\sin(k_z z_s) + A_3\sin(k_z[z_s+2\Delta z]) \\ & +A_4\sin(k_z[z_s+4\Delta z])\big]\left(1-\frac{k_z^2}{k^2}\right)^{\frac{1}{4}} e^{jk_z\frac{dz}{2}}.\end{aligned} \tag{A.10}$$

With this starter field, MMPE outputs pressure, radial velocity, and vertical velocity for a horizontal dipole source.

List of References

[1] J. W. S. Rayleigh, *Theory of Sound Volume I*, 1st ed. London: MacMillan, 1877, pp. 111–117.

[2] T. J. Deal and K. B. Smith, "Modeling acoustic vector fields for inverse problems," in *Proc. 2016 IEEE/OES China Ocean Acoustics (COA)*, 2016, pp. 1–5, doi:10.1109/COA.2016.7535811.

[3] F. B. Jensen, W. A. Kuperman, M. B. Porter, and H. Schmidt, *Computational Ocean Acoustics*, 2nd ed. New York: Springer, 2011, ch. 5, pp. 337–455.

[4] K. B. Smith, "Validating range-dependent, full-field models of the acoustic vector field in shallow water environments," *J. Comp. Acoust.*, vol. 16, no. 4, pp. 471–486, 2008.

[5] D. D. Ellis and D. M. F. Chapman, "A simple shallow water propagation model including shear wave effects," *J. Acoust. Soc. Am.*, vol. 78, no. 6, pp. 2087–2095, 1985.

[6] K. B. Smith, "Convergence, stability, and variability of shallow water acoustic predictions using a split-step Fourier parabolic equation model," *J. Comp. Acoust.*, vol. 9, no. 1, pp. 243–285, 2001.

[7] A. Tolstoy, K. Smith, and N. Maltsev, "The SWAM'99 workshop – an overview," *J. Comp. Acoust.*, vol. 9, no. 1, pp. 1–16, 2001.

[8] K. Case, "Structural acoustics: a general form of reciprocity principles," Mitre Corp, Tech. Rep. JSR-92-193, 1993.

[9] F. B. Jensen, W. A. Kuperman, M. B. Porter, and H. Schmidt, *Computational Ocean Acoustics*, 2nd ed. New York: Springer, 2011, ch. 2, pp. 147–148.

[10] L. E. Kinsler, A. R. Frey, A. B. Coppens, and J. V. Sanders, *Fundamentals of Acoustics*, 4th ed. Hoboken, NJ: Wiley, 2000, pp. 140–142.

[11] A. Haug, R. D. Graves, and H. Überall, "Normal-mode theory of underwater sound propagation from directional multipole sources," *J. Acoust. Soc. Am.*, vol. 56, no. 2, pp. 387–391, 1974.

[12] S. N. Vecherin, D. K. Wilson, and V. E. Ostashev, "Incorporating source directionality into outdoor sound propagation calculations," *J. Acoust. Soc. Am.*, vol. 130, no. 6, pp. 3608–3622, 2011.

THIS PAGE INTENTIONALLY LEFT BLANK

Initial Distribution List

1. Defense Technical Information Center
   Ft. Belvoir, Virginia

2. Dudley Knox Library
   Naval Postgraduate School
   Monterey, California